Journal of Medicinal Chemistry

Article

pubs.acs.org/jmc

Discovery of (*R*,*E*)-*N*-(7-Chloro-1-(1-[4-(dimethylamino)but-2-enoyl]azepan-3-yl)-1*H*-benzo[*d*]imidazol-2-yl)-2-methylisonicotinamide (EGF816), a Novel, Potent, and WT Sparing Covalent Inhibitor of Oncogenic (L858R, ex19del) and Resistant (T790M) EGFR Mutants for the Treatment of EGFR Mutant Non-Small-Cell Lung Cancers

Gérald Lelais,*[,†] Robert Epple,[†] Thomas H. Marsilje,[†] Yun O. Long,[†] Matthew McNeill,[†] Bei Chen,[†] Wenshuo Lu,[†] Jaganmohan Anumolu,[‡] Sangamesh Badiger,[§] Badry Bursulaya,[†] Michael DiDonato,[†] Rina Fong,[†,∥] Jose Juarez,[†] Jie Li,[†] Mari Manuia,[†] Daniel E. Mason,[†] Perry Gordon,[†] Todd Groessl,[†] Kevin Johnson,[†] Yong Jia,[†] Shailaja Kasibhatla,[†] Chun Li,[†] John Isbell,[†] Glen Spraggon,[†] Steven Bender,[†] and Pierre-Yves Michellys[†]

[†]Genomics Institute of the Novartis Research Foundation, 10675 John J. Hopkins Drive, San Diego, California 92121, United States

[‡]Aurigene Discovery Technologies, Bollaram Road, Miyapur, Hyderabad 500 049, India

[§]Aurigene Discovery Technologies, 39-40, Electronic City Phase 2, Bangalore 560 100, India

Supporting Information

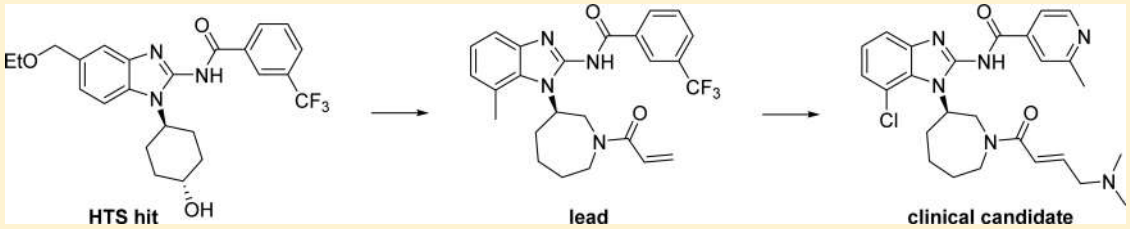

ABSTRACT: Over the past decade, first and second generation EGFR inhibitors have significantly improved outcomes for lung cancer patients with activating mutations in EGFR. However, both resistance through a secondary T790M mutation at the gatekeeper residue and dose-limiting toxicities from wild-type (WT) EGFR inhibition ultimately limit the full potential of these therapies to control mutant EGFR-driven tumors and new therapies are urgently needed. Herein, we describe our approach toward the discovery of **47** (EGF816, nazartinib), a novel, covalent mutant-selective EGFR inhibitor with equipotent activity on both oncogenic and T790M-resistant EGFR mutations. Through molecular docking studies we converted a mutant-selective high-throughput screening hit (**7**) into a number of targeted covalent EGFR inhibitors with equipotent activity across mutants EGFR and good WT-EGFR selectivity. We used an abbreviated in vivo efficacy study for prioritizing compounds with good tolerability and efficacy that ultimately led to the selection of **47** as the clinical candidate.

INTRODUCTION

Inhibitors of epidermal growth factor receptor (EGFR), such as erlotinib (**1**), gefitinib (**2**), and afatinib (**3**) (Figure 1) deliver high objective response rates and increased overall survival (OS) for non-small-cell lung cancer (NSCLC) patients with oncogenic EGFR mutation cancers (i.e., exon 19 deletions or exon 21 L858R single-point mutation).[1−3] However, upon continuous treatment, patients become resistant and, in 50−60% of cases, develop a secondary T790M mutation at the gatekeeper residue of EGFR.[4,5] Evidence suggests that this modification does not block inhibitor binding but rather confers resistance by increasing affinity to ATP.[6]

To overcome drug resistance caused by the T790M mutation, several irreversible pan-EGFR inhibitors belonging to the same structural class as their reversible counterparts (4-anilinoquinazolines) have been developed.[7−11] These include afatinib (**3**)[7] (Figure 1), dacomitinib (**4**)[8,9] (Figure 1), and ceritinib.[10] Their mode of action (MoA) relies on the inactivation of EGFR by forming a covalent bond between an electrophilic Michael acceptor and a conserved cysteine (Cys797) near the ATP binding domain,[12] leading to a more complete and sustained inhibition of the target. Although **3** showed promise in preclinical models of T790M,[7] it is lacking efficacy in the clinic as a single agent for patients with T790M mutation[13] and is unable to achieve an efficacious concentration due to dose-limiting WT EGFR-driven toxicities (e.g., GI-tox and rash).[7,14]

More recently, a new class of mutant-selective irreversible EGFR inhibitors containing an anilinopyrimidine core has been

Received: December 22, 2015
Published: July 19, 2016

DOI: 10.1021/acs.jmedchem.5b01985
J. Med. Chem. 2016, 59, 6671−6689

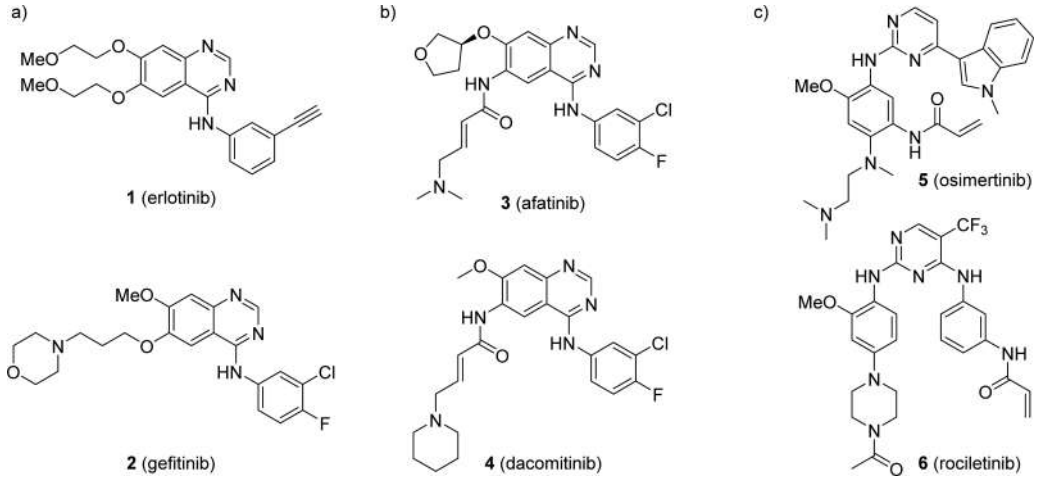

Figure 1. Structures of selected EGFR inhibitors: (a) reversible pan-EGFR inhibitors; (b) irreversible pan-EGFR inhibitors; (c) irreversible mutant-selective EGFR inhibitors.

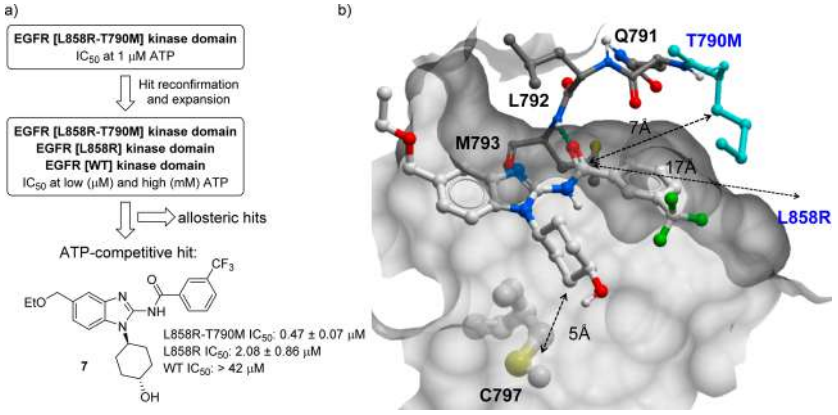

Figure 2. (a) High throughput screening (HTS) approach that culminated in the identification of both allosteric and ATP-competitive EGFR hits. Biochemical IC_{50} (μM) of ATP-competitive hit **7** as average of at least duplicate measurements assessed at 10 μM ATP concentration for either mutants (L858R and L858R-T790M) and WT EGFR constructs. (b) Docking model for the binding of **7** in the ATP-pocket of EGFR T790M-AEE788 cocrystal structure (PDB code 2jiu).[6]

described in the literature.[15−22] Importantly, these inhibitors have low nanomolar activity on EGFR-T790M mutant cells and demonstrate good selectivity toward WT EGFR. On November 13, 2015, osimertinib (AZD9291, **5**)[20,23] (Figure 1) was granted accelerated approval by FDA[24] and rociletinib (CO-1686, **6**)[25,26] (Figure 1) was in pivotal registration trials. Although more clinical data are required, both compounds have the potential to overcome EGFR-T790M resistance mutations while reducing WT EGFR-driven toxicities.[23,25−28]

In this article we report the discovery of **47** (EGF816, nazartinib), a potent covalent mutant-selective EGFR inhibitor with a unique structural motif, currently being evaluated in a number of clinical trials for the treatment of NSCLC.[29−31]

RESULTS AND DISCUSSION

Hit Identification and Modeling. Our strategy for identifying mutant-selective EGFR inhibitors started with a HTS campaign against the EGFR L858R-T790M kinase domain using a homogeneous time-resolved fluorescence (HTRF) based biochemical assay.[32] To achieve maximal inhibitory sensitivity, the compounds were profiled at 1 μM ATP concentrations (ATP $K_m \approx 2$ μM) in single point inhibition. The hits were then reconfirmed with IC_{50} curves at both 1 μM and 1000 μM ATP allowing for the identification of both ATP and non-ATP competitive hits. This communication focuses on the identification of ATP-competitive hits, and the latter ones will be discussed in a separate publication. To further assess the compound's selectivity, we used biochemical counterscreens against EGFR L858R and WT EGFR kinase constructs. Compounds with good activity on EGFR L858R-T790M and selectivity against WT EGFR were considered to be good starting points for further optimization. Activity on EGFR L858R was deemed beneficial but not necessary for hit selection, as we hoped to increase EGFR L858R activity during the hit-to-lead process (vide infra). Among the identified hits, compound **7** displayed an interesting profile, with submicromolar activity on the L858R-T790M construct and selectivity against WT EGFR (Figure 2), and its rather uncommon, but not unprecedented,[33−36] hinge binding motif further stimulated our interest. In fact, although there are a number of aminobenzimidazoles targeting IRAK4[33,34] and ITK,[35] analogue **7** was the only mutant EGFR inhibitor not derived from an aminopyrimidine core, making it a unique structural motif in the EGFR field. Docking of **7** into the active site of EGFR T790M (PDB code 2jiu)[6] revealed a similar binding mode to what had been reported in the literature for IRAK-4 and ITK kinases. It showed a hydrogen bond between the amide carbonyl group of **7** and the hinge-NH of Met793, with the meta-trifluorobenzamide group extending

DOI: 10.1021/acs.jmedchem.5b01985
J. Med. Chem. 2016, 59, 6671−6689

Scheme 1[a]

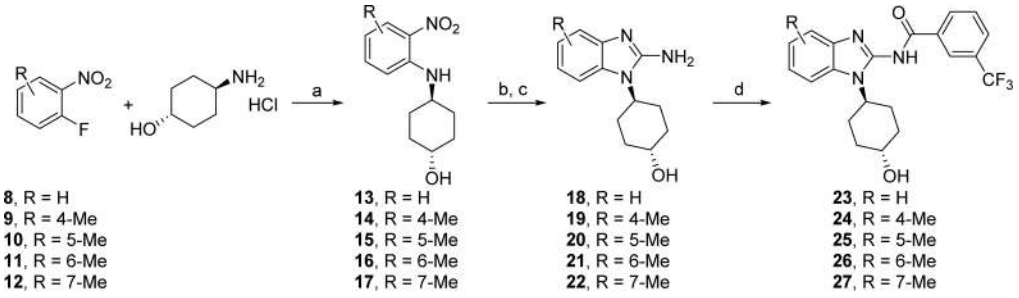

[a]Reagents and conditions: (a) DMF, DIPEA, 120 °C; (b) Pd/C, H_2, MeOH; (c) CNBr, MeCN/H_2O/MeOH 55 °C; (d) 3-(trifluoromethyl)benzoic acid, HATU, DIPEA, DMF or 3-(trifluoromethyl)benzoic acid, HOBt, EDCI, Et_3N, DMF.

Scheme 2[a]

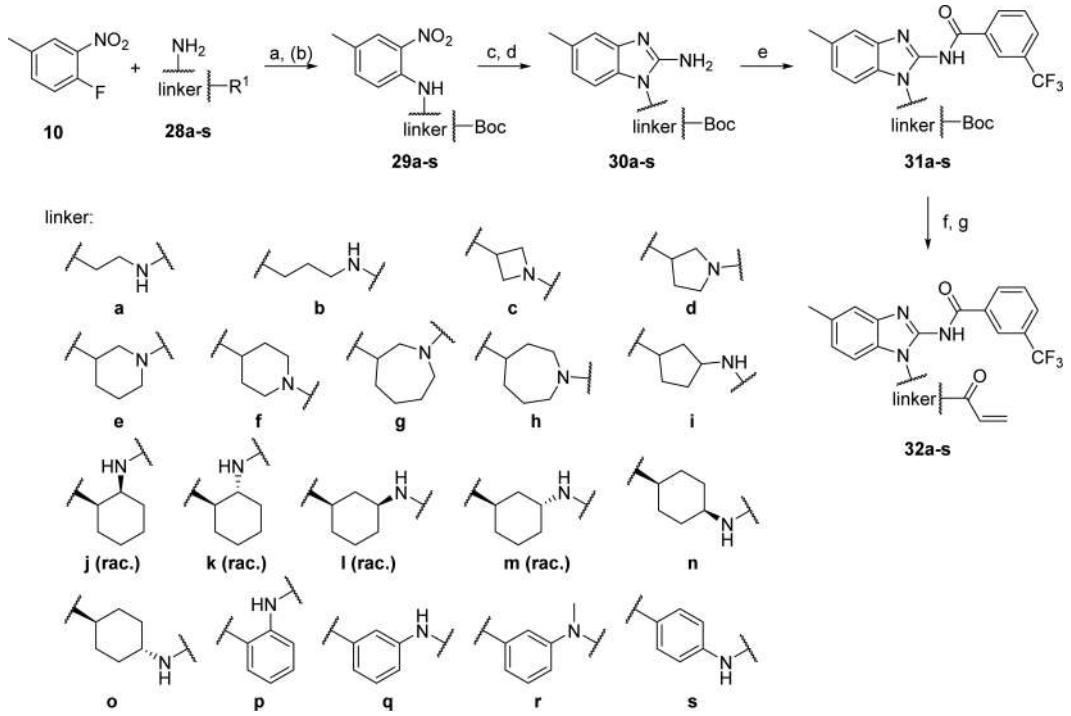

[a]Reagents and conditions: (a) R^1 = Boc: DMF, base (DIPEA or K_2CO_3), 110−130 °C; R^1 = H: neat or DMF, 130−150 °C. (b) For **p**, **q**, **s**, R^1 = H: Boc_2O, Et_3N, dioxane. (c) Pd/C, H_2, MeOH; (d) CNBr, MeCN/H_2O/MeOH 45−50 °C; (e) 3-(trifluoromethyl)benzoic acid, HATU, DIPEA, DMF; (f) TFA, CH_2Cl_2; (g) acryloyl chloride, with or without Et_3N, CH_2Cl_2, 0−20 °C.

toward the methionine gatekeeper residue (Met790) and the cyclohexanol group projecting toward the lip of the ATP-pocket's Cys797 (Figure 2), a residue that had been successfully targeted by irreversible EGFR inhibitors.[7,11,37,38] With this information in hand, we evaluated the structure−activity relationship (SAR) of reversible analogs with the goal of identifying potent ATP-competitive EGFR inhibitors. At the same time, we rationalized that converting mutant-selective ATP-competitive hits into targeted covalent inhibitors would provide compounds with retained selectivity against WT EGFR, with the added benefit of more complete target inhibition as it had been first demonstrated with the identification of the mutant-selective EGFR inhibitor *N*-(3-((5-chloro-2-((2-methoxy-4-(4-methylpiperazin-1-yl)phenyl)amino)pyrimidin-4-yl)oxy)phenyl)-acrylamide (WZ4002).[15]

Chemistry. Compounds were prepared from commercially available 1-fluoro-2-nitroarenes according to the general procedures described in Schemes 1−3. S_NAr reaction with primary amines or appropriately protected diamines followed by nitro reduction and cyclization with cyanogen bromide afforded 2-aminobenzimidazole intermediates **18**−**22**, **30a**−**s**, **37**, or **38** in moderate yields (14−85% over several steps). Amide coupling of **18**−**22**, **30a**−**s**, or **37** with 3-(trifluoromethyl)benzoic acid provided **23**−**27** (Scheme 1) or intermediates **31a**−**s** and **39**, respectively. The latter were deprotected and transformed to the desired products **32a**−**s** (Scheme 2) or **43** and **44** (Scheme 3), in acceptable yields (17−71%). Amide coupling of **37** and **38** with 2-substituted isonicotinic acids afforded **40**−**42** that were deprotected and further coupled with (*E*)-4-(dimethylamino)-but-2-enoic acid to provide **45**−**47** in moderate yields (35−61%, Scheme 3).

In Vitro SAR. The docking of **7** in the kinase domain revealed the solvent exposed nature of the ethoxymethyl group. The lack of stabilizing interactions with the protein provided a rationale for investigating simpler benzimidazole core substitutions as shown in Table 1. As expected, the unsubstituted

DOI: 10.1021/acs.jmedchem.5b01985
J. Med. Chem. 2016, 59, 6671−6689

Scheme 3[a]

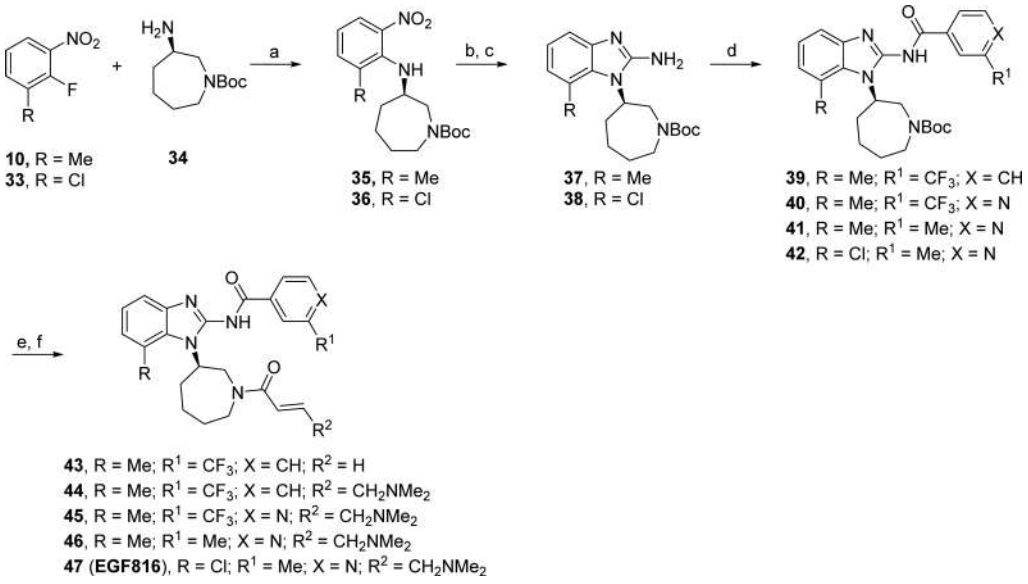

[a]Reagents and conditions: (a) neat, DMA or DMF, DIPEA, 110−140 °C. (b) For **35**: Pd/C, H_2, MeOH. For **36**: Zn, AcOH, room temperature. (c) CNBr, MeCN/H_2O/MeOH 55 °C; (d) acid, HATU, Et_3N, CH_2Cl_2 or acid, HATU, DIPEA, DMF; (e) TFA, CH_2Cl_2 or HCl, dioxane/MeOH. (g) For **43**: acryloyl chloride, CH_2Cl_2, 0−20 °C. For **44**−**47**: (*E*)-4-(dimethylamino)but-2-enoic acid hydrochloride, HOBt, EDCI, Et_3N, DMF or (*E*)-4-(dimethylamino)but-2-enoic acid, HATU, Et_3N, CH_2Cl_2.

Table 1. Structure−Activity Relationship of Benzimidazole Core[a]

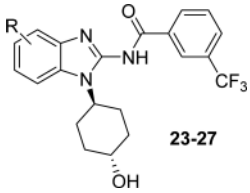

compd	R	L858R-T790M	L858R	WT
23	H	0.26 ± 0.07	2.00 ± 0.41	>50
24	4-Me	1.37 ± 0.56	11.75 ± 5.22	>50
25	5-Me	0.14 ± 0.10	>8.48	>11.78
26	6-Me	0.28 ± 0.12	>16	>50
27	7-Me	0.09 ± 0.01	0.68 ± 0.07	5.27 ± 2.42

[a]Biochemical IC_{50} (μM) assessed at 10 μM ATP concentration for either mutants (L858R and L858R-T790M) and WT EGFR constructs. All data are an average of at least duplicate measurements.

derivative **23** was well tolerated, demonstrating 2-fold improved biochemical activity on the L858R-T790M construct. Comparable potency was observed with the 6-methyl analogue (**26**), while slight potency improvements were noted with compounds that had a methyl substitution at positions 5 and 7 (**25** and **27**). Conversely, as predicted by modeling, compound **24** was less potent, likely due to the methyl group pointing toward the hinge binding domain of EGFR. Importantly, in all cases, selectivity against WT EGFR was maintained, and hints of activity on the oncogenic L858R mutant were observed with **23** and **27**.

Unfortunately, all attempts to further improve the potency of these ATP-competitive hits resulted in little success. A number of amide and cyclohexanol replacements were prepared, none of which resulted in potency improvements (data not shown). Nonetheless, the exquisite WT EGFR selectivity observed in the biochemical assays prompted us to investigate the possibility of adding a well-placed Michael acceptor capable of reacting with Cys797 and result in a targeted covalent inhibitor that could demonstrate improved potency on the mutant EGFR but retain WT EGFR selectivity. As such, compounds of Table 2 were synthesized and a broad variety of lengths and geometries around the reactive thiol of Cys797 were interrogated.

The inhibitory activity of compounds **32a−s** was assessed against the L858R-T790M biochemical construct at 0 and 90 min enzyme/compound preincubation. We employed 90 min preincubation times based on time dependent inhibition studies of irreversible EGFR inhibitors to ensure maximal inhibition of covalent inhibitors (data not shown). These assays were carried out in the presence of 1 mM ATP to simulate physiological intracellular levels of ATP. Importantly, striking differences in EGFR L858R-T790M inactivation were observed, with few linkers (compounds **32b**, **32e**, **32g**, **32l**, **32m**, **32q**, and **32r**) capable of inhibiting the enzyme at nanomolar ranges after a 90 min preincubation and only compound **32g**, with a racemic 3-substituted azepane linker, demonstrating submicromolar activity without preincubation. With these data in hand, we further profiled the most active compounds in various cellular target modulation assays of oncogenic (e.g., H3255, HCC827), resistance (e.g., H1975), and WT (e.g., HaCaT) EGFR settings as shown in Table 3. The cellular potency on H1975 was in good agreement with the biochemical inhibitory concentration on the L858R-T790M construct, with **32g** demonstrating superior activity (IC_{50} = 0.006 μM), followed by **32e** (IC_{50} = 0.02 μM; *R*-enantiomer). In addition, compound **32g** was highly potent across all mutant EGFR lines and displayed acceptable WT EGFR selectivity (≥50-fold).

Intrigued by the initial observation that 7-methyl derivative **27** displayed a preferred substitution pattern, we prepared both enantiomers of the 7-methyl analogue of **32g**. Interestingly, the *R*-enantiomer **43** demonstrated very good activity across mutants cell lines with acceptable WT EGFR selectivity (≥25-fold, Table 4), whereas the *S*-enantiomer was >200-fold

DOI: 10.1021/acs.jmedchem.5b01985
J. Med. Chem. 2016, 59, 6671−6689

Table 2. Structure–Activity Relationship of the Linker Region Aimed at Identifying the Optimal Length and Geometry for Covalent Bond to Cys797[a]

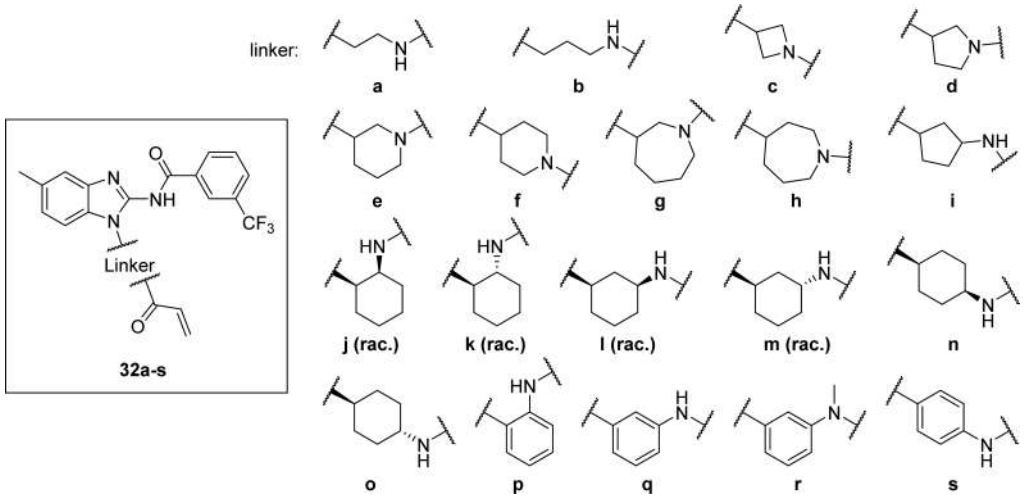

compd	0 min	90 min	compd	0 min	90 min
32a	>50	>50	**32k**	>50	>50
32b	>50	0.05 ± 0.008	**32l**	>50	0.004 ± 0.001
32c	>50	>50	**32m**	>50	0.06 ± 0.05
32d	>50	>50	**32n**	>50	>50
32e	>50	0.02 ± 0.002	**32o**	>50	>50
32f	>37.67	16.46 ± 7.86	**32p**	>50	>32.77
32g	0.83 ± 0.14	<0.002	**32q**	>50	0.004 ± 0.002
32h	>50	>50	**32r**	22.31 ± 24.75	0.01 ± 0.003
32i	>50	6.81 ± 1.88	**32s**	>50	>50
32j	>50	>50			

[a]Biochemical IC_{50} (μM) assessed with or without a 90 min preincubation of compound and EGFR L858R-T790M enzyme at 1 mM ATP concentrations using HTRF assay as described in the methods section. All data are an average of at least duplicate measurements.

Table 3. Activity Profiles of 32b, 32e, 32g, 32l, 32m, 32q, 32r, and Reference Compounds 5 and 6 from Patient-Derived Cell Lines H1975 (EGFR L858R-T790M), H3255 (EGFR L858R), and HCC827 (EGFR Del E746-A750) and the Immortalized Human Keratinocyte Cell Line HaCaT (WT EGFR)[a]

compd	H1975	H3255	HCC827	HaCaT
32b	525 ± 126.4	>10000	1653 ± 717	>10000
32e[b]	24.7 ± 5.3	421 ± 139.3	153 ± 29.4	>10000
32g	6.1 ± 2.0	74.9 ± 31.9	15.9 ± 1.9	4330 ± 779
32l[c]	41.4 ± 8.7	543 ± 0.195	ND	>10000
32m[c]	409 ± 338	>3716	ND	>10000
32q	134.8 ± 29.3	1041 ± 327	272.1 ± 48.5	>10000
32r	181 ± 45.3	660 ± 169.1	267.5 ± 48.1	>10000
5	2.5 ± 0.7	4.1 ± 1.4	2.5 ± 0.5	73.7 ± 16.6
6	4.1 ± 1.4	13.8 ± 3.2	9.5 ± 0.9	262.3 ± 79.9

[a]Target modulation IC_{50} values (nM) were determined after a 3 h compound treatment to the cells. All data are an average of at least duplicate measurements. [b]Cellular IC_{50} values for the active *R*-enantiomer, obtained after chiral HPLC separation (see Supporting Information). [c]Data for **32l** and **32m** are from engineered NIH-3T3 cells of the corresponding L858R-T790M, L858R, or WT-EGFR mutants.

less potent across assays (H1975 IC_{50} = 401 nM, H3255 IC_{50} = 3125 nM, HCC827 IC_{50} = 863 nM, HaCaT $IC_{50} \geq 10\,000$ nM).

To gain confidence that these analogues were indeed binding to EGFR L858R-T790M via a covalent bond to Cys797, we performed crystallization studies with a variety of mutant and WT EGFR constructs. The structures of **43** bound to either WT EGFR or the T790M single mutant were determined and exhibit an overall structure consistent with a kinase in the active conformation, DFG-in and intact salt bridge to helix-C. Comparison of the two **43**-bound structures revealed nearly identical binding site residues and compound conformations (Figure 3B) and hence did not provide any clues that could explain the observed selectivity toward the T790M mutant versus the WT enzyme. However, examining the apo structures of both the WT enzyme (PDB code 2gs2)[39] and the T790M mutant (PDB code 2jit)[6] revealed a network of water molecules bound to the hinge region of the WT enzyme that is not present in the apo structure of the T790M mutant (Figure 3A). In the WT apo structure, the Thr790 side chain mediates a hydrogen bonding interaction to two water molecules that are also coordinated to the backbone of several residues in the hinge region (Ala743, Gln791, and Leu788). In addition, there is a third water molecule coordinated to the backbone amide of Met793. These three water molecules are absent in the apo T790M mutant structure and are instead replaced by two loosely coordinated water molecules that interact with the DFG aspartic acid side chain, Asp855 (Figure 3A). In the compound-bound structures (Figure 3B), analogue **43** is covalently linked to Cys797 and makes a hydrogen bonding interaction to the backbone amide NH of Met793. Binding of the compound to the WT enzyme requires the displacement of the three strongly coordinated water molecules present in this region. We hypothesize that the cost of displacing these water molecules that are

DOI: 10.1021/acs.jmedchem.5b01985
J. Med. Chem. 2016, 59, 6671–6689

Table 4. In Vitro and in Vivo Profile of Select Mutant-Selective EGFR Inhibitors

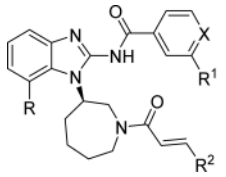

43, R = Me; R^1 = CF_3; X = CH; R^2 = H
44, R = Me; R^1 = CF_3; X = CH; R^2 = CH_2NMe_2
45, R = Me; R^1 = CF_3; X = N; R^2 = CH_2NMe_2
46, R = Me; R^1 = Me; X = N; R^2 = CH_2NMe_2
47, R = Cl; R^1 = Me; X = N; R^2 = CH_2NMe_2

	43	44	45	46	47
H1975 IC_{50}[a] (nM)	1.39 ± 0.03	2.18 ± 0.75	1.51 ± 0.01	2.11 ± 0.17	4.18 ± 0.03
H3255 IC_{50}[a] (nM)	14.84 ± 0.91	45.90 ± 15.78	2.65 ± 0.07	3.05 ± 0.14	6.11 ± 0.08
HCC827 IC_{50}[a] (nM)	3.93 ± 2.03	12.45 ± 5.91	1.48 ± 0.56	1.01 ± 0.33	1.52 ± 0.08
HaCaT IC_{50}[a] (nM)	249.6 ± 94.0	351.0 ± 240.4	72.0 ± 15.5	68.0 ± 22.8	160.6 ± 12.8
H1975 LipE	3.65	3.13	4.59	4.83	4.30
HT-sol., pH 6.8 (μM)	<2	10.5	12.7	>175	>175
CYP3A4 IC_{50}[a]	3.5	22.2	>25	>25	>25
CYP2D6 IC_{50}[a]	>25	16.7	6.1	>25	7
CYP2C9 IC_{50}[a]	3.4	17.6	>25	>25	>25
human CL_{int}[b]	83	49	71	26	34
mouse CL_{int}[b]	245	233	96	62	66
mouse iv CL (mL min^{-1} kg^{-1})	54.0	57.2	62.5	68.5	31.6
mouse po AUC (h·nM)[c]	808	4391	2839	3527	12789
mouse *F* (%)	6	40	27	34	60

[a]All IC_{50} data given in μM unless otherwise noted and are an average of at least duplicate measurements. [b]CL_{int} is intrinsic clearance in liver microsomes, μL min^{-1} mg^{-1}. [c]AUC from 20 mg/kg oral dose to male balb/c mice. **43** and **45** were formulated in 0.5% methylcellulose and 0.5% Tween 80 suspension. **44** was formulated in solution containing 75% PEG300 and 25% D5W (5% dextrose in water). **46** was formulated in solution containing 5% ethanol, 30% PEG300, and 65% Solutol (20%), and **47** was formulated in a solution containing 5% ethanol, 25% PEG300, and 70% D5W (5% dextrose in water).

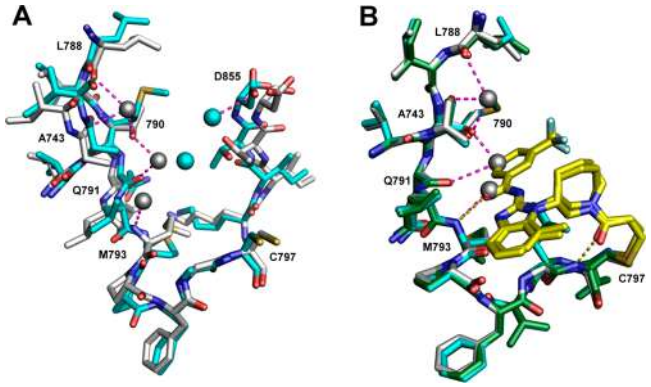

Figure 3. Comparison of apo and drug bound hinge region. (A) Superposition of apo WT EGFR (white sticks, PDB code 2gs2)[39] and EGFR T790M mutant (cyan sticks, PDB code 2jit).[6] Water molecules associated with the WT structure are shown in gray spheres; those associated with the T790M structure are shown in cyan spheres. Polar interaction is depicted by magenta dotted line. (B) Superposition of the apo WT EGFR (white sticks, PDB code 2gs2),[39] WT EGFR-**43** complex (green sticks, PDB code 5fed), and EGFR T790M-**43** complex (cyan sticks, PDB code 5fee). Polar interactions are depicted by yellow dotted line. In both drug bound structures, **43** is shown in yellow sticks.

not present in the T790M apo structure may lead to the observed selectivity profile of **43**.

Although **43** demonstrated promising cellular activity, it had very low aqueous solubility (<2 μM) and poor ADME and PK properties. It is a moderate inhibitor of CYP3A4 and 2C9 with an IC_{50} of ∼3.5 μM. It also has high intrinsic microsomal clearance,[40] especially in rodents, which correlated with high in vivo clearance (CL) in mice. The high in vitro liver metabolism and poor solubility resulted in only 6% oral bioavailability in mice (Table 4). In vitro metabolism study in mouse, rat, and human liver microsomes showed that oxidation of 7-methyl groups and oxidation of acrylate groups are the two main metabolic pathways (Figure S1 in Supporting Information). To modulate the compound's reactivity, we first investigated a number of Michael acceptors similar to those reported in the literature.[37,38] Amino-substituted crotonamides had been identified as optimal groups for a number of covalent pan-EGFR inhibitors (e.g., afatinib, dacomitinib, neratinib). The dimethylamino crotonamide analogue **44** retained comparable activity to **43** in H1975, but it was consistently a few fold less potent toward cell lines with oncogenic mutations (H3255 and HCC827). Conversely, it demonstrated measurable improvements in solubility and metabolic stability (Table 4) and resulted in increased oral exposure and bioavailability in mice. Additionally, the amino-substituted crotonamide resulted in improved CYP inhibition profiles with IC_{50} > 10 μM for CYP3A4 and 2C9.

Next, we sought to improve the compound's lipophilic efficiency (LipE)[41] and explore opportunities to increase activity on the oncogenic mutations while maintaining good WT EGFR selectivity. As the only difference between mutants resides at the gatekeeper residue, we investigated the SAR of the trifluorobenzamide group. In general, (hetero)alkyl and (hetero)cycloalkyl groups led to complete loss in activity (data not shown), whereas heteroaromatic groups were tolerated. In particular, the trifluoromethylpiridyl **45** demonstrated single digit nM activity on H1975 and was nearly equipotent on the activating mutations, resulting in a 10-fold potency improvement compared to **44**. It is important to note that increased potency was also observed on HaCaT but to a lesser extent than the L858R and L858R-T790M mutant cell lines. From docking and X-ray cocrystallization structures (vide infra) we believe the reason for improved activity on oncogenic and WT EGFR cell lines results from the displacement of one of the conserved water molecules by the pyridine group, with the nitrogen serving as

DOI: 10.1021/acs.jmedchem.5b01985
J. Med. Chem. 2016, 59, 6671−6689

a)

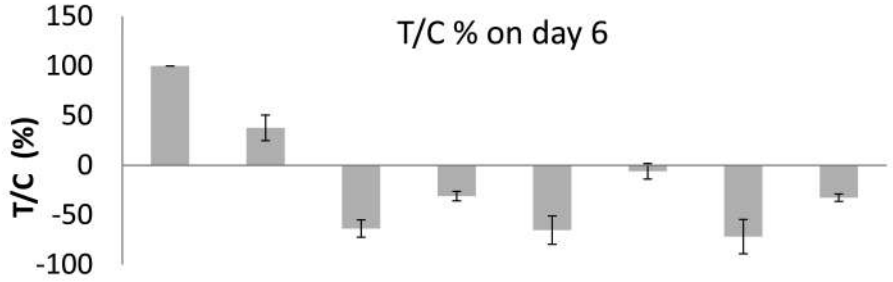

	vehicle	afatinib	**45**	**45**	**46**	**46**	**47**	**47**
Dose (mg/kg)		25	50	20	50	20	50	25
T/C (%)	100	38	-64	-31	-65	-6	-72	-32
H1975 IC_{50} (nM)		4	1	1	2	2	3	3
Δ (%body weight)	+3.9	-2.4	-3.5	-0.3	-5.0	-1.1	+3.8	+5.3

b)

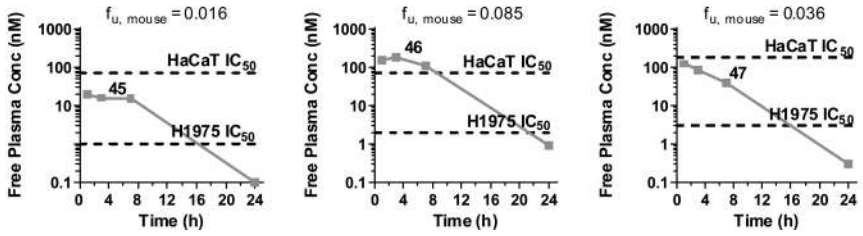

Figure 4. (a) Mouse H1975 abbreviated efficacy study. Compounds were dosed po q.d. for 5 days. Δ % body weights were recorded on day 5, and percent mean tumor volume of the drug-treated group versus mean tumor volume of the control group (T/C) was measured at end of study (day 6). (b) End of study free plasma exposure of compounds **45**−**47** for 50 mg/kg dose. Plasma PK samples were collected on day 5 at 30 min, 3 h, 7 h, and 24 h postdosing.

H-bond acceptor and interacting with Thr854. The difference in the extent of increased activity toward oncogenic versus WT EGFR cell lines may be due to the difference in ATP K_m between enzymes and because the oncogenic mutations are constitutively active, whereas WT EGFR is in equilibrium between active and inactive forms.[6,42]

Although solubility was slightly improved, **45** was still relatively insoluble (12.7 μM HT-sol. at pH 6.8). Replacing the trifluoromethyl functionality by a methyl group resulted in **46**, a compound with comparable potency across mutants EGFR and selectivity against WT EGFR but with much improved water solubility (>175 μM HT-sol. at pH 6.8). Both derivatives had relatively high in vivo clearance in mice and low to moderate oral bioavailability (Table 4). As mentioned above, one of the main metabolic soft spots was the 7-methyl group. Replacing this residue by a chloro group led to analogue **47**. Gratifyingly, **47** had single digit activity on the mutant cell lines (4, 6, 2 nM IC_{50} in H1975, H3255, and HCC827, respectively) with less than 2-fold loss of potency on H3255 compared to **46**. At the same time, it displayed reduced activity on HaCaT (0.18 μM), providing similar WT EGFR selectivity (~36-fold). Importantly, **47** demonstrated improved ADME and PK properties as compared to other compounds.

The chemical reactivity of **43**−**47** and potential for nonspecific covalent binding to proteins were assessed in comparison to afatinib. Upon incubation for 1 h with 10 mM glutathione (GSH) or with human liver microsomes in the presence of NADPH and GSH, compounds **43**−**47** formed only minor GSH adducts (<5%). In contrast, afatinib showed high level of GSH conjugate (60%). The much reduced reactivity of **43**−**47** toward GSH suggests a lower risk of nonspecific covalent binding to proteins.

In Vivo Efficacy Studies for Compound Selection. An integrated approach evaluating PK, tolerability, and efficacy was incorporated into the in vivo studies for compound selection. As such, **45**−**47** were profiled in a short-term in vivo efficacy study using a H1975 mouse xenograft model and compared to afatinib as positive control (Figure 4). In short, H1975 tumor cells were inoculated subcutaneously in Foxn1 female nude mice. Mice were then randomized into groups of 5 animals and dosed orally once daily for 5 days at 50 and 20 mg/kg or 25 mg/kg once tumors reached 150−200 mm^3. Afatinib was dosed at maximum tolerated dose of 25 mg/kg. Body weight was measured daily and change in tumor volume compared to control (T/C) was assessed on days 4 and 6. Plasma samples were collected after last dose on day 5, and exposures of each compound were determined. Afatinib demonstrated tumor growth inhibition with 38% T/C, consistent with what was reported in the literature.[7] All other compounds demonstrated dose-dependent efficacy with near complete regression at the highest dose tested (50 mg/kg), and free drug concentrations in plasma were well above their in vitro IC_{50} values for at least 14 h within each dosing interval. Compound **47** was very well tolerated with body weight gains comparable to vehicle at both doses. On the other hand, **45** and **46** displayed up to 5% body weight loss.

DOI: 10.1021/acs.jmedchem.5b01985
J. Med. Chem. 2016, 59, 6671−6689

Table 5. In Vivo PK Parameters of 47 in Mouse, Rat, and Dog

	mouse		rat		dog	
parameter	iv[a]	po[a]	iv[a]	po[a]	iv[b]	po[c]
dose (mg/kg)	5	20	3	10	1	10
CL (mL min^{-1} kg^{-1})	31.6		15.7		43.7	
V_{ss} (L/kg)	2.8		2.4		35.2	
MRT (h)	1.5		2.6		13.8	
AUC (h·nM)	5343	12786	6527	11951	783	5230
C_{max} (nM)		2938		987		435
T_{max} (h)		0.83		3.0		2.3
F (%)		60		55		67

[a]Free base formulated in a solution of 5% ethanol, 25% PEG300, and 70% D5W (5% dextrose in water). [b]HCl salt formulated in a solution of 100% D5W (5% dextrose in water). [c]HCl salt formulated in a solution of 0.5% (w/v) aqueous methylcellulose and 0.5% Tween 80.

For this reason, compound **47** was further profiled in preclinical in vivo PK studies in mouse, rat, and dog (Table 5). The compound showed moderate volume of distribution and low to moderate clearance in rodents (30% and 35% of rat and mouse liver blood flow, respectively). In the dog, **47** showed high clearance and high volume of distribution. The high clearance in dog was consistent with higher in vitro dog microsomal clearance and higher fraction unbound in dog plasma as compared to other species. In contrast, the human liver microsomal CL of **47** is relatively low, and the compound is predicted to have favorable human PK profile with low to moderate clearance and good oral exposure.

On the basis of these results, analogue **47** was selected for further profiling as described by Jia et al.[43] and was ultimately nominated as our clinical candidate after confirming adequate safety profile (Tables S2−S4).

Compound 47 and Close Analogue 46 Covalently Bind to Cys797. Attempts to cocrystallize **47** with various EGFR constructs have not yet been successful. Instead, we obtained cocrystals of the close analogue **46** with the EGFR T790M construct that confirmed the covalent bond to Cys797 (Figure 5a). The covalent nature of **47** with EGFR L858R and EGFR T790M-L858R mutant constructs was assessed by mass spectrometry (Figure 5b,c). Incubation of **47** with both EGFR constructs resulted in one main product per protein that had an average mass 495 Da higher than the unmodified protein. This was consistent with addition of one molecule of **47** to the protein on average. LC/MS/MS of the enzymatic digests identified adducts of **47** that localized to Cys797 and Cys775. Spectral counting was used for relative comparison of adduction; 96% of MS/MS acquired for Cys797 was identified as modified with **47** (96 out of 100 spectra), while only 0.3% of Cys775 was modified (1 out of 324 spectra). The relative number of **47**-modified to total spectra for the two cysteines suggested that Cys797 is the main site of **47** modification.

CONCLUSIONS

We have described the identification of a novel, covalent, mutant-selective EGFR inhibitor with nearly equipotent activity on both oncogenic (L858R and ex19del) and T790M-resistant mutations and good selectivity over WT EGFR. From a high-throughput screen, we converted a reversible mutant-selective EGFR hit (**7**) into an irreversible inhibitor lead (**43**) by carefully investigating the linker length and geometry necessary to engage

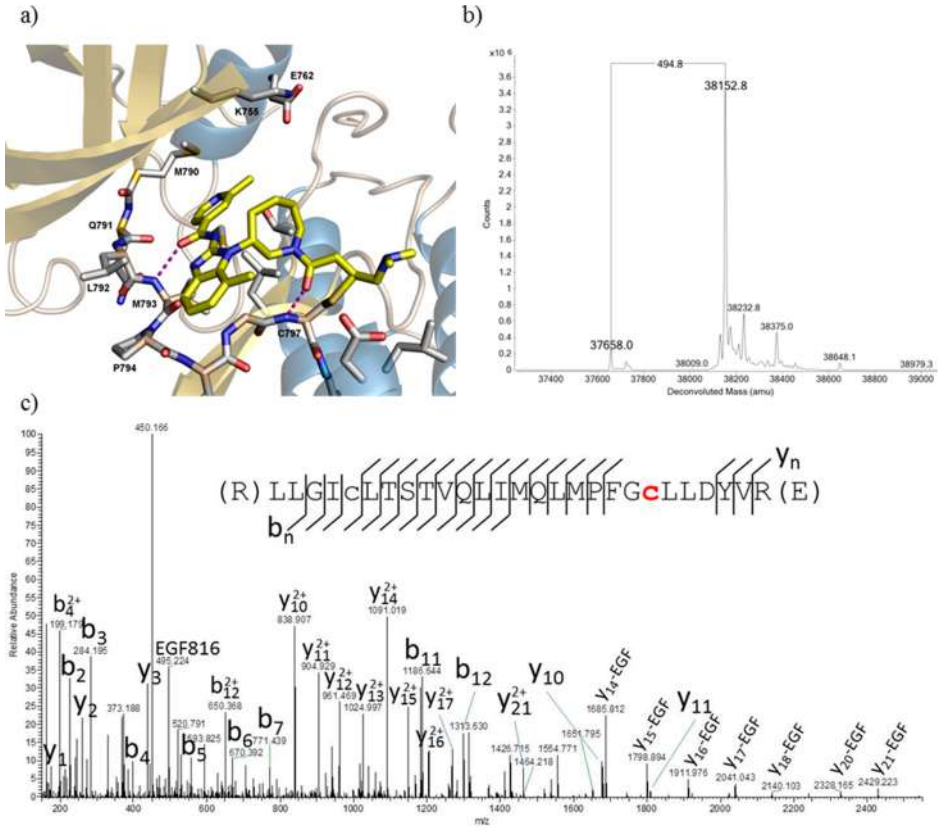

Figure 5. Compounds **46** and **47** bind irreversibly to EGFR constructs: (a) cocrystal structure of EGFR T790M-**46** complex; (b) deconvoluted mass spectrum of EGFR L858R-T790M after in vitro incubation with **47**; (c) MS/MS of EGFR peptide covalently modified with **47** at Cys797.

DOI: 10.1021/acs.jmedchem.5b01985
J. Med. Chem. 2016, 59, 6671−6689

Cys797. Molecular docking and metabolite identification experiments were used to increase potency on cell lines with oncogenic mutations while retaining adequate WT EGFR selectivity. Finally, we employed an abbreviated in vivo efficacy study to select **47** for further profiling and ultimately as the clinical candidate. Compound **47** is currently being tested in numerous clinical trials,[29−31] and it has already demonstrated encouraging efficacy in NSCLC patients with T790M mutations. As previously disclosed, efficacy was seen across all dose levels with an overall response rate of 60% and a disease control rate of 93% in early assessments.[44] Full results from clinical trials will be reported in due course.

EXPERIMENTAL PROCEDURES

Unless otherwise noted, materials were obtained from commercial suppliers and were used without further purification. Removal of solvent under reduced pressure or concentration refers to distillation using Büchi rotary evaporator attached to a vacuum pump (3 mmHg). Products obtained as solids or high boiling oils were dried under vacuum (1 mmHg).

Purification of compounds by preparative RP-HPLC was achieved using a Waters autopurification system consisting of a 2767 autosampler/fraction collector, a 2525 binary gradient module, a 2487 UV detector, and a ZQ mass spectrometer. Compounds were purified using flow rate of 30 mL/min with a 50 mm × 20 mm i.d. Ultra 120 5 μm C18Q column (Peeke Scientific, Novato, CA). A 7.5 min linear gradient from 10% solvent A (acetonitrile with 0.035% trifluoroacetic acid) in solvent B (water with 0.05% trifluoroacetic acid) to 30−90% A was used, followed by a 2.5 min hold at 90% A. Silica gel chromatography was performed by CombiFlash (separation system Sg. 100c, ISCO). Elemental analyses were carried out by Midwest Microlabs LLC, Indianapolis, IN. ^{1}H NMR spectra were recorded on Bruker XWIN-NMR (400 MHz) spectrometer. Proton resonances are reported in parts per million (ppm) downfield from tetramethylsilane (TMS). ^{1}H NMR data are reported as multiplicity (s, singlet; d, doublet; t, triplet; q, quartet; dd, doublet of doublets; dt, doublet of triplets; br s, broad singlet). For spectra obtained in $CDCl_3$, DMSO-d_6, CD_3OD, CD_3CN the residual protons (7.27, 2.50, 3.31, and 1.94 ppm, respectively) were used as the internal reference. In general, peaks associated with the azepane and (hetero)aromatic rings display two distinct sets of peaks (approximately 50:50 intensity) in spectra acquired at 300 K (atropoisomers). The peaks collapse to a single set at higher temperature (383 K) (see Figures S2 and S3 for ^{1}H and ^{13}C NMR spectra of **47**). Optical rotations were measured at the sodium D line, using an ATAGO POLAX-2L polarimeter and a 100 mm cell at 23 °C and are reported as follows: concentration (c = g/100 mL), solvent.

Purity of Compounds. All final compounds were analyzed with a Waters ZQ 2000 LC/MS system, which used an Agilent binary pump or Shimadzu LC10 and Agilent photodiode array detector (PDA) along with a Sedere 75 evaporative light scattering detector (ELSD). Samples were injected from 96-well or 384-well plates with a Leap Technologies HTS Pal autosampler. The mobile phases used were (A) H_2O + 0.05% TFA and (B) acetonitrile + 0.05% TFA. A gradient HPLC method with flow of 1.0 mL/min started at 5% B, with a hold of 0.1 min before a linear increase to 90% B at 2.60 min. At 2.71 min the B mobile phase was increased to 100% and held until 2.98 min before returning to 5% B at 2.99 min. Total run time was 3.0 min. The column was re-equilibrated in the time between injections. The column used was a Waters Atlantis dC18 2.1 mm × 30 mm, 3 μm. The mass spectrometer was operated in positive mode, with a spray voltage of 3.2 kV and cone voltage of 30 V. The source and desolvation temperatures were 130 and 400 °C, respectively, with 600 L/h of nitrogen desolvation flow. The progress of reactions and the purity of products were measured using 254 and 214 nm wavelengths and electrospray ionization (ESI) positive or negative mode. Mass spectra were obtained in ESI positive or negative mode. All of the final compounds were found to be >95% when analyzed at either the 254 or 214 nm wavelengths. Chiral compounds were also analyzed by chiral HPLC or chiral SFC and demonstrated to have at least 95% ee.

General Procedure for the Synthesis of Compounds 13−17, 29a−o, 29r, 35, and 36. A solution of the desired 1-fluoro-2-nitroarene **8−12** or **33** (1−1.5 equiv) in a suitable solvent, such as DMF or DMA (0.2−0.8 M), or neat was treated with the requisite amine (1 equiv) and a base such as DIPEA or K_2CO_3 (1.5−4 equiv), and the reaction mixture was warmed to 110−140 °C for 2−16 h. The reaction mixture was then cooled to room temperature and partitioned between water and EtOAc. The aqueous layer was extracted twice more with EtOAc, and the pooled extracts were washed consecutively with water and brine, dried over Na_2SO_4, filtered, and concentrated under reduced pressure. The residue was purified by silica gel chromatography to afford the desired nitroanilines (**13−17**, **29a−o**, **29r**, **35**, and **36**).

***trans*-4-((2-Nitrophenyl)amino)cyclohexan-1-ol (13).** Yield, 69%.

***trans*-4-((3-Methyl-2-nitrophenyl)amino)cyclohexan-1-ol (14).** Yield, 54%. ^{1}H NMR (DMSO-d_6, 400 MHz): δ 11.98 (s, 1H), 7.26 (t, J = 8.3 Hz, 1H), 6.85 (d, J = 8.3 Hz, 1H), 6.54 (d, J = 7.3 Hz, 1H), 6.08 (d, J = 7.9 Hz, 1H), 4.58 (m, 1H), 3.42 (m, 1H), 2.29 (s, 3H), 2.15 (m, 2H), 1.95 (m, 2H), 1.82 (m, 2H), 1.25 (m, 2H). MS calculated for $C_{13}H_{17}N_2O_3$ $(M - H)^-$ 249.13, found 249.0.

***trans*-4-((4-Methyl-2-nitrophenyl)amino)cyclohexan-1-ol (15).** Yield, 35%. ^{1}H NMR ($CDCl_3$, 400 MHz): δ 7.97 (s, 1H), 7.25 (d, J = 8.3 Hz, 1H), 6.78 (d, J = 8.8 Hz, 1H), 3.82 (m, 1H), 3.45 (m, 1H), 2.25 (s, 3H), 2.21 (m, 2H), 2.05 (m, 2H), 1.52 (m, 4H). MS calculated for $C_{13}H_{17}N_2O_3$ $(M - H)^-$ 249.13, found 248.9.

***trans*-4-((5-Methyl-2-nitrophenyl)amino)cyclohexan-1-ol (16).** Yield, 68%. ^{1}H NMR ($CDCl_3$, 400 MHz): δ 8.05 (d, J = 7.5 Hz, 1H), 6.61 (s, 1H), 6.42 (d, J = 7.5 Hz, 1H), 3.78 (m, 1H), 3.45 (m, 1H), 2.35 (s, 3H), 2.15 (m, 4H), 1.55 (m, 4H). MS calculated for $C_{13}H_{19}N_2O_3$ $(M + H)^+$ 251.13, found 251.3.

***trans*-4-((2-Methyl-6-nitrophenyl)amino)cyclohexan-1-ol (17).** Yield, 68%. ^{1}H NMR (DMSO-d_6, 400 MHz): δ 7.78 (d, J = 7.4 Hz, 1H), 7.45 (d, J = 6.9 Hz, 1H), 6.89 (t, J = 7.8 Hz, 1H), 6.13 (d, J = 9.8 Hz, 1H), 4.54 (d, J = 4.4 Hz, 1H), 3.38 (m, 1H), 3.33 (m, 1H), 2.32 (s, 3H), 1.77 (m, 4H), 1.19 (m, 4H). MS calculated for $C_{13}H_{19}N_2O_3$ $(M + H)^+$ 251.13, found 251.2.

***tert*-Butyl (2-((4-Methyl-2-nitrophenyl)amino)ethyl)-carbamate (29a).** Yield, 43%.

***tert*-Butyl (3-((4-Methyl-2-nitrophenyl)amino)propyl)-carbamate (29b).** Yield, 45%. MS calculated for $C_{15}H_{24}N_3O_4$ $(M + H)^+$ 310.18, found 310.2.

***tert*-Butyl 3-((4-Methyl-2-nitrophenyl)amino)azetidine-1-carboxylate (29c).** Yield, 56%. ^{1}H NMR (DMSO-d_6, 400 MHz): δ 8.05 (s, 1H), 8.01 (s, 1H), 7.30 (d, J = 7.9 Hz, 1H), 6.44 (d, J = 8.3 Hz, 1H), 4.38 (m, 2H), 4.32 (m, 1H), 3.87 (m, 2H), 2.29 (s, 3H), 1.46 (s, 9H). MS calculated for $C_{15}H_{21}N_3O_4$ $(M + H)^+$ 308.15, found 308.3.

***tert*-Butyl 3-((4-Methyl-2-nitrophenyl)amino)pyrrolidine-1-carboxylate (29d).** Yield, 66%.

***tert*-Butyl 3-((4-Methyl-2-nitrophenyl)amino)piperidine-1-carboxylate (29e).** Yield, 65%. MS calculated for $C_{17}H_{26}N_3O_4$ $(M + H)^+$ 336.19, found 336.1.

***tert*-Butyl 4-((4-Methyl-2-nitrophenyl)amino)piperidine-1-carboxylate (29f).** Yield, 78%.

***tert*-Butyl 3-((4-Methyl-2-nitrophenyl)amino)azepane-1-carboxylate (29g).** Yield, 93%. MS calculated for $C_{18}H_{28}N_3O_4$ $(M + H)^+$ 350.21, found 350.1.

***tert*-Butyl 4-((4-Methyl-2-nitrophenyl)amino)azepane-1-carboxylate (29h).** Yield, 88%. ^{1}H NMR ($CDCl_3$, 400 MHz): δ 8.04 (d, J = 7.3 Hz, 1H), 7.98 (s, 1H), 6.70 (d, J = 8.8 Hz, 1H), 3.21−3.75 (m, 5H), 2.31 (s, 3H), 1.61−2.05 (m, 6H), 1.53 (s, 9H). MS calculated for $C_{18}H_{28}N_3O_4$ $(M + H)^+$ 350.20, found 350.2.

***tert*-Butyl (3-((4-Methyl-2-nitrophenyl)amino)cyclopentyl)-carbamate (29i).** Yield, 54%. MS calculated for $C_{17}H_{26}N_3O_4$ $(M + H)^+$ 336.19, found 336.2.

***tert*-Butyl *cis*-(2-((4-Methyl-2-nitrophenyl)amino)-cyclohexyl)carbamate (29j).** Yield, 53%. ^{1}H NMR ($CDCl_3$, 400 MHz): δ 8.31 (d, J = 8.3 Hz, 1H), 7.98 (s, 1H), 7.22 (d, J = 8.8 Hz, 1H), 6.85 (d, J = 8.8 Hz, 1H), 4.55−4.75 (m, 1H), 3.98−4.18 (m, 1H),

DOI: 10.1021/acs.jmedchem.5b01985
J. Med. Chem. 2016, 59, 6671−6689

3.75–3.95 (m, 1H), 2.25 (s, 3H), 1.45–1.81 (m, 8H), 1.39 (s, 9H). MS calculated for $C_{18}H_{28}N_3O_4$ $(M + H)^+$ 350.20, found 350.2.

***tert*-Butyl *trans*-(2-((4-Methyl-2-nitrophenyl)amino)-cyclohexyl)carbamate (29k).** Yield, 54%. ^{1}H NMR ($CDCl_3$, 400 MHz): δ 8.17 (d, J = 7.4 Hz, 1H), 7.96 (s, 1H), 7.24 (d, J = 8.3 Hz, 1H), 6.87 (d, J = 8.8 Hz, 1H), 4.4–4.5 (m, 1H), 3.31–3.75 (m, 2H), 2.25 (s, 3H), 2.05–2.21 (m, 4H), 1.22–1.85 (m, 4H), 1.25 (s, 9H). MS calculated for $C_{18}H_{28}N_3O_4$ $(M + H)^+$ 350.20, found 350.2.

***tert*-Butyl *cis*-(3-((4-Methyl-2-nitrophenyl)amino)-cyclohexyl)carbamate (29l).** Yield, 46%. ^{1}H NMR (DMSO-d_6, 400 MHz): δ 7.86 (s, 1H), 7.79 (d, J = 8.0 Hz, 1H), 7.38 (d, J = 8.4 Hz, 1H), 7.07 (d, J = 8.8 Hz, 1H), 6.83 (d, J = 7.6 Hz, 1H), 3.66–3.64 (m, 1H), 3.41–3.37 (m, 1H), 2.22 (s, 3H), 2.11 (d, J = 11.2 Hz, 1H), 1.95 (d, J = 12.0 Hz, 1H), 1.80–1.71 (m, 2H), 1.37 (s, 9H), 1.23–1.05 (m, 1H). MS calculated for $C_{18}H_{28}N_3O_4$ $(M + H)^+$ 350.21 found 350.1.

***tert*-Butyl *trans*-(3-((4-Methyl-2-nitrophenyl)amino)-cyclohexyl)carbamate (29m).** Yield, 34%. ^{1}H NMR ($CDCl_3$, 400 MHz): δ 7.86 (s, 1H), 7.79 (d, J = 7.8 Hz, 1H), 7.38 (d, J = 8.3 Hz, 1H), 7.07 (d, J = 8.8 Hz, 1H), 6.84 (d, J = 7.8 Hz, 1H), 3.55–3.75 (m, 1H), 3.31–3.42 (m, 1H), 2.22 (s, 3H), 1.62–2.19 (m, 4H), 1.45 (s, 9H), 1.05–1.25 (m, 4H). MS calculated for $C_{18}H_{28}N_3O_4$ $(M + H)^+$ 350.20, found 350.1.

***tert*-Butyl *cis*-(4-((4-Methyl-2-nitrophenyl)amino)-cyclohexyl)carbamate (29n).** Yield, 62%. ^{1}H NMR ($CDCl_3$, 400 MHz): δ 8.25 (br s, 1H), 8.15 (s, 1H), 7.25 (d, J = 9.3 Hz, 1H), 6.77 (d, J = 8.8 Hz, 1H), 4.45–4.61 (m, 1H), 3.51–3.79 (m, 2H), 2.26 (s, 3H), 1.65–1.95 (m, 8H), 1.45 (s, 9H).

***tert*-Butyl *trans*-(4-((4-Methyl-2-nitrophenyl)amino)-cyclohexyl)carbamate (29o).** Yield, 78%. ^{1}H NMR (DMSO-d_6, 400 MHz): δ 7.85 (s, 1H), 7.80 (d, J = 7.8 Hz, 1H), 7.35 (d, J = 7.5 Hz, 1H), 7.12 (d, J = 7.9 Hz, 1H), 6.81 (d, J = 7.5 Hz, 1H), 3.41–3.58 (m, 1H), 3.19–3.31 (m, 1H), 2.21 (s, 3H), 1.75–2.15 (m, 4H), 1.41 (s, 9H), 1.21–1.45 (m, 4H).

***tert*-Butyl Methyl(3-((4-methyl-2-nitrophenyl)amino)-phenyl)carbamate (29r).** Yield, 33%. ^{1}H NMR (DMSO-d_6, 400 MHz): δ 9.17 (s, 1H), 7.93 (s, 1H), 7.38–7.05 (m, 6H), 3.18 (s, 3H), 2.27 (s, 3H), 1.39 (s, 9H). MS calculated for $C_{19}H_{22}N_3O_4$ $(M - H)^-$ 356.16, found 356.2.

***(R)*-*tert*-Butyl 3-((2-Methyl-6-nitrophenyl)amino)azepane-1-carboxylate (35).** Yield, 60%. ^{1}H NMR ($CDCl_3$, 400 MHz): δ 7.93–7.87 (m, 1H), 7.37–7.31 (m, 1H), 6.91–6.79 (m, 1.5H), 6.50–6.47 (m, 0.5H), 3.88–3.76 (m, 2H), 3.57–3.52 (m, 1H), 3.22–2.78 (m, 2H), 2.43–2.41 (m, 3H), 1.92–1.60 (m, 5H), 1.47–1.38 (m, 10H). MS calculated for $C_{18}H_{28}N_3O_4$ $(M + H)^+$ 350.20, found 350.0. $[\alpha]_D^{23}$ +71.42° (c 0.420, MeOH).

***(R)*-*tert*-Butyl 3-((2-Chloro-6-nitrophenyl)amino)azepane-1-carboxylate (36).** Yield, 54%. ^{1}H NMR ($CDCl_3$, 400 MHz): δ 8.00–7.91 (m, 1H), 7.58–7.49 (m, 1H), 7.02–6.51 (m, 2H), 4.31–4.03 (m, 1H), 3.84–2.98 (m, 4H), 1.98–1.60 (m, 5H), 1.46–1.39 (m, 10H). MS calculated for $C_{17}H_{25}ClN_3O_4$ $(M + H)^+$ 370.15, found 370.10. $[\alpha]_D^{23}$ −95.06° (c 0.263, MeOH).

General Procedure for the Synthesis of Compounds 29p–q and 29s. Synthesis of *tert*-Butyl (3-((4-Methyl-2-nitrophenyl)-amino)phenyl)carbamate (29q). A 100 mL round-bottom flask was charged with 1-fluoro-4-methyl-2-nitrobenzene (3.4 g, 22.08 mmol) and 1,3-phenylenediamine (2.0 g, 18.40 mmol), and the neat mixture was warmed to 150 °C for 3 h. The reaction mixture was dissolved in CH_2Cl_2 and purified by silica gel chromatography: 0–30% EtOAc/hexanes gradient. The resulting N^1-(4-methyl-2-nitrophenylbenzene-1,3-diamine was dissolved in 1,4-dioxane (10 mL) and treated with $(Boc)_2O$ (4.66 g, 21.3 mmol) and Et_3N (4.4 mL, 31.8 mmol). The red solution was stirred for 24 h at room temperature and then diluted with CH_2Cl_2 (100 mL) and washed with water. The resulting organic layer was separated, dried over anhydrous Na_2SO_4, and concentrated under reduced pressure to a viscous red residue, which was purified by silica gel chromatography (0–30% EtOAc/hexanes gradient) to afford *tert*-butyl (3-((4-methyl-2-nitrophenyl)amino)phenyl)carbamate **29q** (1.5 g, 20%). MS calculated for $C_{18}H_{20}N_3O_4$ $(M - H)^-$ 342.15, found 342.1.

***tert*-Butyl (2-((4-Methyl-2-nitrophenyl)amino)phenyl)-carbamate (29p).** Yield, 22%. MS calculated for $C_{18}H_{20}N_3O_4$ $(M - H)^-$ 342.15, found 342.1.

***tert*-Butyl (4-((4-Methyl-2-nitrophenyl)amino)phenyl)-carbamate (29s).** Yield, 31%. ^{1}H NMR (DMSO-d_6, 400 MHz): δ 9.41 (br s, 1H), 9.24 (s, 1H), 7.91 (s, 1H), 7.49 (d, J = 8.8 Hz, 2H), 7.31 (dd, J = 9.8 Hz, 2.0 Hz, 1H), 7.21 (d, J = 8.8 Hz, 2H), 6.99 (d, J = 8.8 Hz, 1H), 2.25 (s, 3H), 1.47 (s, 9H).

General Procedure for the Synthesis of Compounds 18–22, 30a–s, and 37. Synthesis of *trans*-4-(2-Amino-1*H*-benzo[*d*]-imidazol-1-yl)cyclohexan-1-ol (18). A solution of **13** (350 mg, 1.48 mmol) in methanol (15 mL) was degassed with nitrogen, treated with Pd/C (55 mg, 15.7 mol %), and then stirred under H_2 atmosphere for 1 h. The reaction mixture was filtered through Celite, the Celite rinsed with MeOH (40 mL), and the filtrate concentrated under reduced pressure to afford a crude residue, which was dissolved in water (1 mL) and added to a solution of cyanogen bromide (185 mg, 1.75 mmol) in MeOH/MeCN (3:1, 4 mL). The reaction mixture was then warmed to 50 °C for 2 h, cooled to 0 °C, treated with saturated aqueous Na_2CO_3 to pH 10, and then stirred for 30 min while warming to room temperature. The resulting suspension was filtered and dried under high vacuum to afford **18** (280 mg, 77%). ^{1}H NMR (DMSO-d_6, 400 MHz): δ 7.33 (d, J = 7.8 Hz, 1H), 7.11 (d, J = 7.4 Hz, 1H), 6.91 (t, J = 7.4 Hz, 1H), 6.82 (t, J = 7.8 Hz, 1H), 6.34 (br s, 2H), 4.58–4.67 (m, 1H), 4.15–4.24 (m, 1H), 3.55–3.73 (m, 1H), 2.11–2.35 (m, 2H), 1.85–2.01 (m, 2H), 1.31–1.51 (m, 2H).

***trans*-4-(2-Amino-4-methyl-1*H*-benzo[*d*]imidazol-1-yl)-cyclohexan-1-ol (19).** Yield, 26%.

***trans*-4-(2-Amino-5-methyl-1*H*-benzo[*d*]imidazol-1-yl)-cyclohexan-1-ol (20).** Yield, 91%. ^{1}H NMR (DMSO-d_6, 400 MHz): δ 7.17 (d, J = 7.8 Hz, 1H), 6.91 (s, 1H), 6.63 (d, J = 8.3 Hz, 1H), 6.20 (br s, 2H), 4.65 (m, 1H), 4.15 (m, 1H), 2.65 (m, 1H), 2.28 (s, 3H), 2.21 (m, 2H), 1.85 (m, 2H), 1.65 (m, 2H), 1.41 (m, 2H). MS calculated for $C_{14}H_{20}N_3O$ $(M + H)^+$ 246.15, found 246.2.

***trans*-4-(2-Amino-6-methyl-1*H*-benzo[*d*]imidazol-1-yl)-cyclohexan-1-ol (21).** Yield, 67%. ^{1}H NMR (DMSO-d_6, 400 MHz): δ 7.13 (s, 1H), 6.98 (d, J = 7.9 Hz, 1H), 6.71 (d, J = 7.9 Hz, 1H), 6.18 (br s, 2H), 4.68 (br s, 1H), 4.15 (m, 1H), 3.65 (m, 1H), 2.33 (s, 3H), 2.11 (m, 2H), 1.95 (m, 2H), 1.66 (m, 2H), 1.42 (m, 2H). MS calculated for $C_{14}H_{20}N_3O$ $(M + H)^+$ 246.15, found 246.1.

***trans*-4-(2-Amino-7-methyl-1*H*-benzo[*d*]imidazol-1-yl)-cyclohexan-1-ol (22).** Yield, 33%. ^{1}H NMR (DMSO-d_6, 400 MHz): δ 6.95 (d, J = 7.9 Hz, 1H), 6.80 (t, J = 7.3 Hz, 1H), 6.61 (d, J = 7.4 Hz, 1H), 5.97 (br s, 2H), 4.55 (m, 1H), 3.63 (m, 1H), 2.57 (s, 3H), 2.26 (m, 2H), 1.95 (m, 2H), 1.72 (m, 2H), 1.35 (m, 2H). MS calculated for $C_{14}H_{20}N_3O$ $(M + H)^+$ 246.15, found 246.1.

***tert*-Butyl (2-(2-Amino-5-methyl-1*H*-benzo[*d*]imidazol-1-yl)-ethyl)carbamate (30a).** Yield, 80%. ^{1}H NMR (DMSO-d_6, 400 MHz): δ 6.98 (d, J = 7.5 Hz, 1H), 6.94 (s, 1H), 6.85 (m, 1H), 6.65 (d, J = 7.5 Hz, 1H), 6.21 (br s, 2H), 3.98 (m, 2H), 3.18 (m, 2H), 2.31 (s, 3H), 1.35 (s, 9H).

***tert*-Butyl (3-(2-Amino-5-methyl-1*H*-benzo[*d*]imidazol-1-yl)-propyl)carbamate (30b).** Yield, 84%. MS calculated for $C_{16}H_{25}N_4O_2$ $(M + H)^+$ 305.20, found 305.2.

***tert*-Butyl 3-(2-Amino-5-methyl-1*H*-benzo[*d*]imidazol-1-yl)-azetidine-1-carboxylate (30c).** Yield, 81%. ^{1}H NMR (DMSO-d_6, 400 MHz): δ 7.12 (d, J = 7.8 Hz, 1H), 7.00 (s, 1H), 6.74 (d, J = 7.8 Hz, 1H), 6.31 (br s, 2H), 5.24 (m, 1H), 4.31 (m, 4H), 2.32 (s, 3H), 1.45 (s, 9H).

***tert*-Butyl 3-(2-Amino-5-methyl-1*H*-benzo[*d*]imidazol-1-yl)-pyrrolidine-1-carboxylate (30d).** Yield, 78%. ^{1}H NMR (DMSO-d_6, 400 MHz): δ 7.04 (d, J = 7.8 Hz, 1H), 6.96 (s, 1H), 6.66 (d, J = 7.9 Hz, 1H), 6.34 (br s, 2H), 4.98 (m, 1H), 3.62 (m, 4H), 2.21 (m, 1H), 2.29 (s, 3H), 2.13 (m, 1H), 1.45 (s, 9H).

***tert*-Butyl 3-(2-Amino-5-methyl-1*H*-benzo[*d*]imidazol-1-yl)-piperidine-1-carboxylate (30e).** Yield, 64%. ^{1}H NMR ($CDCl_3$, 400 MHz): δ 7.24 (s, 1H), 7.17 (d, J = 7.6 Hz, 1H), 6.85 (d, J = 8.0 Hz, 1H), 4.64 (br s, 2H), 4.17 (t, J = 14.8 Hz, 2H), 3.99–3.93 (m, 1H), 3.32 (d, J = 11.6 Hz, 1H), 2.79 (t, J = 12.4 Hz, 1H), 2.41 (s, 3H), 2.38–2.37 (m, 1H), 2.34 (d, J = 3.2 Hz, 1H), 1.91 (d, J = 13.6 Hz, 1H),

DOI: 10.1021/acs.jmedchem.5b01985
J. Med. Chem. 2016, 59, 6671–6689

1.69−1.61 (m, 1H), 1.47 (s, 9H). MS calculated for $C_{18}H_{27}N_4O_2$ $(M + H)^+$ 331.21, found 331.0.

***tert*-Butyl 4-(2-Amino-5-methyl-1*H*-benzo[*d*]imidazol-1-yl)-piperidine-1-carboxylate (30f).** Yield, 72%. ^{1}H NMR (DMSO-d_6, 400 MHz): δ 7.55 (d, J = 7.5 Hz, 1H), 7.41 (m, 2H), 7.07 (s, 1H), 6.86 (d, J = 8.3 Hz, 1H), 4.2−4.4 (m, 1H), 3.82−4.02 (m, 2H), 3.31−3.3.45 (m, 1H), 2.79−3.01 (m, 1H), 2.34 (s, 3H), 2.19−2.38 (m, 1H), 1.78−1.99 (m, 2H), 1.43−1.61 (m, 1H), 1.1 (s, 9H). MS calculated for $C_{18}H_{27}N_4O_2$ $(M + H)^+$ 331.21, found 331.3.

***tert*-Butyl 3-(2-Amino-5-methyl-1*H*-benzo[*d*]imidazol-1-yl)-azepane-1-carboxylate (30g).** Yield, 91%. ^{1}H NMR (DMSO-d6, 400 MHz): δ 7.15−7.12 (m, 1H), 6.93 (s, 1H), 6.66 (d, J = 7.6 Hz, 1H), 6.26 (s, 2H), 4.29 (br s, 1H), 3.81−3.75 (m, 1H), 3.55−3.36 (m, 3H), 2.29 (s, 3H), 2.08 (s, 2H), 1.86−1.68 (m, 5H), 1.40 (s, 9H). MS calculated for $C_{19}H_{29}N_4O_2$ $(M + H)^+$ 345.23, found 345.1.

***tert*-Butyl 4-(2-Amino-5-methyl-1*H*-benzo[*d*]imidazol-1-yl)-azepane-1-carboxylate (30h).** Yield, 94%. MS calculated for $C_{19}H_{29}N_4O_2$ $(M + H)^+$ 345.22, found 345.1.

***tert*-Butyl (3-(2-Amino-5-methyl-1*H*-benzo[*d*]imidazol-1-yl)-cyclopentyl)carbamate (30i).** Yield, 77%. ^{1}H NMR (DMSO-d_6, 400 MHz): δ 12.55 (br s, 1H), 7.93 (br s, 2H), 7.42 (d, J = 8.2 Hz, 1H), 7.21 (d, J = 1.4 Hz, 1H), 6.98 (d, J = 8.2 Hz, 1H), 4.88−4.71 (m, 1H), 3.99−3.79 (m, 1H), 2.40 (s, 3H), 2.25−1.81 (m, 6H), 1.40 (s, 9H).

***tert*-Butyl *cis*-(2-(2-Amino-5-methyl-1*H*-benzo[*d*]imidazol-1-yl)cyclohexyl)carbamate (30j).** Yield, 77%. ^{1}H NMR ($CDCl_3$, 400 MHz): δ 7.19 (s, 1H), 7.10 (d, J = 8.3 Hz, 1H), 6.82 (d, J = 7.8 Hz, 1H), 4.81 (br s, 2H), 4.21−4.39 (m, 1H), 4.01−4.19 (m, 1H), 2.47−2.61 (m, 1H), 2.38 (s, 3H), 1.35−2.12 (m, 6H), 1.05 (s, 9H). MS calculated for $C_{19}H_{29}N_4O_2$ $(M + H)^+$ 345.22, found 345.0.

***tert*-Butyl *trans*-(2-(2-Amino-5-methyl-1*H*-benzo[*d*]imidazol-1-yl)cyclohexyl)carbamate (30k).** Yield, 75%. ^{1}H NMR ($CDCl_3$, 400 MHz): δ 7.32 (d, J = 7.3 Hz, 1H), 7.26 (s, 1H), 7.02 (d, J = 7.8 Hz, 1H), 4.81−4.95 (m, 1H), 4.41−4.50 (m, 1H), 4.01−4.15 (m, 1H), 3.61 (m, 1H), 3.15−3.31 (m, 1H), 2.41 (s, 3H), 1.62−2.19 (m, 4H), 1.11−1.38 (m, 4H), 1.42 (s, 9H). MS calculated for $C_{19}H_{29}N_4O_2$ $(M + H)^+$ 345.22, found 345.0.

***tert*-Butyl *cis*-(3-(2-Amino-5-methyl-1*H*-benzo[*d*]imidazol-1-yl)cyclohexyl)carbamate (30l).** ^{1}H NMR (DMSO-d_6, 400 MHz): δ 7.12 (d, J = 8.0 Hz, 1H), 6.93 (s, 1H), 6.83 (d, J = 7.6 Hz, 1H), 6.66 (t, J = 6.8 Hz, 1H), 6.26 (s, 2H), 4.21 (dd, J = 3.6 Hz, 1H), 3.52−3.31 (m, 1H), 2.28 (s, 3H), 2.07−1.94 (m, 2H), 1.81 (d, J = 10.4 Hz, 2H), 1.66 (d, J = 11.6 Hz, 1H), 1.36 (s, 9H), 1.28−1.20 (m, 3H). MS calculated for $C_{19}H_{29}N_4O_2$ $(M + H)^+$ 345.23, found 345.0.

***tert*-Butyl *trans*-(3-(2-Amino-5-methyl-1*H*-benzo[*d*]imidazol-1-yl)cyclohexyl)carbamate (30m).** Yield, 95%.

***tert*-Butyl *cis*-(4-(2-Amino-5-methyl-1*H*-benzo[*d*]imidazol-1-yl)cyclohexyl)carbamate (30n).** Yield, 98%.

***tert*-Butyl *trans*-(4-(2-Amino-5-methyl-1*H*-benzo[*d*]imidazol-1-yl)cyclohexyl)carbamate (30o).** Yield, 95%. ^{1}H NMR (DMSO-d_6, 400 MHz): δ 7.22 (d, J = 7.8 Hz, 1H), 6.92 (s, 1H), 6.81 (d, J = 7.5 Hz, 1H), 6.41 (d, J = 7.5 Hz, 1H), 6.25 (br s, 2H), 4.15 (m, 1H), 3.41 (m, 1H), 2.35 (s, 3H), 2.21 (m, 2H), 1.95 (m, 2H), 1.85 (m, 2H), 1.41 (s, 9H), 1.39 (m, 2H). MS calculated for $C_{19}H_{29}N_4O_2$ $(M + H)^+$ 345.2, found 345.2.

***tert*-Butyl (2-(2-Amino-5-methyl-1*H*-benzo[*d*]imidazol-1-yl)-phenyl)carbamate (30p).** Yield, 96%. ^{1}H NMR (DMSO-d_6, 400 MHz): δ 8.28 (s, 1H), 7.75 (d, J = 8.2 Hz, 1H), 7.45 (m, 1H), 7.27 (m, 2H), 7.02 (s, 1H), 6.63 (d, J = 7.9 Hz, 1H), 6.47 (d, J = 7.6 Hz, 1H), 5.99 (br s, 2H), 2.32 (s, 3H), 1.45 (s, 9H). MS calculated for $C_{19}H_{23}N_4O_2$ $(M + H)^+$ 339.15, found 339.3.

***tert*-Butyl (3-(2-Amino-5-methyl-1*H*-benzo[*d*]imidazol-1-yl)-phenyl)carbamate (30q).** Yield, 93%. ^{1}H NMR ($CDCl_3$, 400 MHz): δ 7.61(s, 1H), 7.48−7.39 (m, 2H), 7.25 (d, J = 10.4 Hz, 1H), 7.10 (t, J = 1.6 Hz, 1H), 6.95−6.85 (m, 3H), 2.41 (s, 3H), 2.17 (s, 2H), 1.51 (s, 9H). MS calculated for $C_{19}H_{23}N_4O_2$ $(M + H)^+$ 339.18, found 339.1.

***tert*-Butyl (3-(2-Amino-5-methyl-1*H*-benzo[*d*]imidazol-1-yl)-phenyl)(methyl)carbamate (30r).** Yield, 93%. ^{1}H NMR (DMSO-d_6, 400 MHz): δ 7.55 (t, J = 8.0 Hz, 1H), 7.42 (d, J = 8.4 Hz, 1H), 7.37 (s, 1H), 7.24 (d, J = 7.2 Hz, 1H), 7.03 (s, 1H), 6.77 (t, J = 8.4 Hz, 1H), 6.68−6.19 (m, 1H), 6.19 (s, 2H), 3.26 (s, 3H), 2.32 (s, 3H), 1.42 (s, 9H). MS calculated for $C_{20}H_{25}N_4O_2$ $(M + H)^+$ 353.20, found 353.0.

***tert*-Butyl (4-(2-Amino-5-methyl-1*H*-benzo[*d*]imidazol-1-yl)-phenyl)carbamate (30s).** Yield, 80%. ^{1}H NMR (DMSO-d_6, 400 MHz): δ 9.64 (br s, 1H), 7.67 (d, J = 8.3 Hz, 2H), 7.38 (m, 2H), 7.07 (s, 1H), 6.61−6.80 (m, 4H), 2.38 (s, 3H), 1.45 (s, 9H).

***tert*-Butyl (*R*)-3-(2-Amino-7-methyl-1*H*-benzo[*d*]imidazol-1-yl)azepane-1-carboxylate (37).** Yield, 86%. ^{1}H NMR (DMSO-d_6, 400 MHz): δ 6.99 (dd, J = 7.8, 1.2 Hz, 1H), 6.83 (t, J = 7.6 Hz, 1H), 6.72−6.56 (m, 1H), 6.07 (d, J = 20.8 Hz, 2H), 4.84−4.58 (m, 1H), 3.85−3.61 (m, 2H), 3.59−3.47 (m, 1H), 3.36 (dt, J = 16.1, 5.8 Hz, 1H), 2.59 (d, J = 9.2 Hz, 3H), 2.31−2.14 (m, 1H), 1.97−1.69 (m, 5H), 1.44 (s, 5H), 1.32 (s, 4H). MS calculated for $C_{19}H_{29}N_4O_2$ $(M + H)^+$ 345.22, found 345.2. $[\alpha]_D^{23}$ +74.07° (c 0.272, MeOH).

***tert*-Butyl (*R*)-3-(2-Amino-7-chloro-1*H*-benzo[*d*]imidazol-1-yl)azepane-1-carboxylate (38).** A mixture of **36** (7.5 g, 19.5 mmol) and Zn (12.8 g, 195 mmol) in AcOH (22 mL) was stirred at room temperature for 2 h. The reaction was basified with saturated aqueous Na_2CO_3, filtered and the filtrate extracted with EtOAc (3 × 80 mL). The combined organic extracts were washed with brine, dried over Na_2SO_4, and concentrated in vacuo to afford *tert*-butyl (*R*)-3-((2-amino-6-chlorophenyl)amino)azepane-1-carboxylate (6.62 g, 19.48 mmol), which was immediately dissolved in MeOH (200 mL) and treated with a solution of cyanogen bromide (3.09 g, 29.22 mmol) in H_2O (75 mL) and MeCN (75 mL). The reaction mixture was stirred at 50 °C for 6 h, concentrated under reduced pressure, basified with saturated aqueous Na_2CO_3, and then extracted with EtOAc (3 × 90 mL). The combined organic extracts were dried over Na_2SO_4 and concentrated under reduced pressure. The crude material was purified by HPLC to afford **38** (3.3 g, 46%). ^{1}H NMR ($CDCl_3$, 400 MHz): δ 7.34−7.26 (m, 1H), 7.04−6.97 (m, 2H), 6.05−5.85 (m, 1H), 5.84−5.72 (m, 1H), 5.50−5.37 (m, 0.5H), 5.10−4.80 (m, 0.5H), 4.41−4.23 (m, 1H), 4.09−3.96 (m, 0.5H), 3.94−3.81 (m, 1H), 3.76−3.57 (m, 1H), 3.22−3.14 (m, 0.5H), 2.84−2.63 (m, 1H), 2.34−2.17 (m, 1H), 2.07−1.84 (m, 1H), 1.82−1.64 (m, 2H), 1.53 (s, 9H), 1.48−1.37 (m, 1H). MS calculated for $C_{18}H_{26}ClN_4O_2$ $(M + H)^+$ 365.17, found 365.1. $[\alpha]_D^{23}$ +71.17° (c 0.281, MeOH).

General Procedure for the Synthesis of Compounds 23−27, 31a−s, and 39−42. Synthesis of *N*-(1-(*trans*-4-Hydroxycyclohexyl)-1*H*-benzo[*d*]imidazol-2-yl)-3-(trifluoromethyl)-benzamide (23). To a solution of **18** (100 mg, 0.433 mmol) and 3-(trifluoromethyl)benzoic acid (82 mg, 0.433 mmol) in DMF (5 mL) were added HATU (197 mg, 0.519 mmol) and DIPEA (167 mg, 1.30 mmol), and the reaction mixture was stirred at room temperature for 14 h. The reaction mixture was then diluted with water (20 mL), extracted with CH_2Cl_2 (3 × 100 mL), and the pooled organics were washed with water and then brine, dried over Na_2SO_4, filtered, and concentrated under reduced pressure. The material thus obtained was purified by silica gel chromatography (0−2% MeOH in CH_2Cl_2 gradient) to afford **23** (110 mg, 64%). ^{1}H NMR (DMSO-d_6, 400 MHz): δ 12.91 (s, 1H), 8.52 (m, 2H), 7.93 (m, 1H), 7.80 (m, 1H), 7.75 (m, 1H), 7.61 (m, 1H), 7.27 (m, 2H), 4.79 (m, 2 H), 3.72 (m, 1H), 2.59 (m, 2H), 2.06 (d, J = 10.4 Hz, 2H), 1.84 (d, J = 12.4, 2H), 1.49 (m, 2H). MS calculated for $C_{21}H_{21}F_3N_3O_2$ $(M + H)^+$ 404.16, found 403.9.

***N*-(1-(*trans*-4-Hydroxycyclohexyl)-4-methyl-1*H*-benzo[*d*]-imidazol-2-yl)-3-(trifluoromethyl)benzamide (24).** Yield, 20%. ^{1}H NMR (DMSO-d_6, 400 MHz): δ 12.44 (s, 1H), 8.49 (m, 2H), 7.92 (m, 1H), 7.77 (m, 1H), 7.58 (d, J = 7.6 Hz, 1H), 7.20 (m, 1H), 7.09 (d, J = 8.0 Hz, 1H), 4.76 (m, 2H), 3.68 (m, 1H), 2.51 (m, 2H), 2.50 (s, 3H), 2.02 (d, J = 10.4 Hz, 2H), 1.81 (d, J = 11.2 Hz, 2H), 1.46 (m, 2H). MS calculated for $C_{22}H_{23}F_3N_3O_2$ $(M + H)^+$ 418.17, found 418.0.

***N*-(1-(*trans*-4-Hydroxycyclohexyl)-5-methyl-1*H*-benzo[*d*]-imidazol-2-yl)-3-(trifluoromethyl)benzamide (25).** Yield, 18%. ^{1}H NMR (DMSO-d_6, 400 MHz): δ 12.79 (s, 1H), 8.48 (m, 2H), 7.89 (d, J = 7.2 Hz, 1H), 7.75 (t, J = 8.0 Hz, 1H), 7.58 (d, J = 8.4 Hz, 1H), 7.38 (s, 1H), 7.07 (d, J = 8.0 Hz, 1H), 4.75 (m, 2H), 3.68 (m, 1H), 2.61 (m, 2H), 2.39 (s, 3H), 2.02 (d, J = 10.4 Hz, 2H),

DOI: 10.1021/acs.jmedchem.5b01985
J. Med. Chem. 2016, 59, 6671−6689

1.79 (d, J = 11.2 Hz, 2H), 1.43 (m, 2H). MS calculated for $C_{22}H_{23}F_3N_3O_2$ $(M + H)^+$ 418.17, found 418.2.

***N*-(1-(*trans*-4-Hydroxycyclohexyl)-6-methyl-1*H*-benzo[*d*]-imidazol-2-yl)-3-(trifluoromethyl)benzamide (26).** Yield, 54%. ^{1}H NMR (DMSO-d_6, 400 MHz): δ 12.79 (s, 1H), 8.48 (m, 2H), 7.90 (d, J = 7.2 Hz, 1H), 7.75 (t, J = 8.0 Hz, 1H), 7.54 (s, 1H), 7.45 (d, J = 8.0 Hz, 1H), 7.05 (d, J = 8.4 Hz, 1H), 4.77 (m, 1H), 4.74 (br s, 1H), 3.70 (m, 1H), 2.56 (m, 2H), 2.43 (s, 3H), 2.03 (d, J = 10.0 Hz, 2H), 1.79 (d, J = 10.8 Hz, 2H), 1.46 (m, 2H). MS calculated for $C_{22}H_{23}F_3N_3O_2$ $(M + H)^+$ 418.17, found 418.1.

***N*-(1-(*trans*-4-Hydroxycyclohexyl)-7-methyl-1*H*-benzo[*d*]-imidazol-2-yl)-3-(trifluoromethyl)benzamide (27).** Yield, 39%. ^{1}H NMR (DMSO-d_6, 400 MHz): δ 12.93 (s, 1H), 8.52 (s, 1H), 8.43 (d, J = 7.6 Hz, 1H), 7.90 (d, J = 7.6 Hz, 1H), 7.77 (t, J = 7.6 Hz, 1H), 7.46 (d, J = 7.2 Hz, 1H), 7.12 (t, J = 7.2 Hz, 1H), 7.03 (d, J = 7.2 Hz, 1H), 4.76 (m, 1H), 4.74 (br s, 1H), 3.64 (m, 1H), 3.00 (q, J = 12.0 Hz, 2H), 2.71 (s, 3H), 2.03 (d, J = 10.4 Hz, 2H), 1.89 (d, J = 11.6 Hz, 2H), 1.41 (m, 2H). MS calculated for $C_{22}H_{23}F_3N_3O_2$ $(M + H)^+$ 418.17, found 418.2.

***tert*-Butyl (2-(5-Methyl-2-(3-(trifluoromethyl)benzamido)-1*H*-benzo[*d*]imidazol-1-yl)ethyl)carbamate (31a).** Yield, 68%. ^{1}H NMR (DMSO-d_6, 400 MHz): δ 12.69 (br s, 1H), 8.54 (d, J = 7.8 Hz, 1H), 8.48 (s, 1H), 7.88 (d, J = 7.3 Hz, 1H), 7.73 (t, J = 5.4 Hz, 1H), 7.71 (t, J = 7.9 Hz, 1H), 7.38 (m, 1H), 7.08 (d, J = 7.8 Hz, 1H), 6.86 (br s, 1H), 4.28 (m, 2H), 3.37 (m, 2H), 2.39 (s, 3H), 1.25 (s, 9H).

***tert*-Butyl (3-(5-Methyl-2-(3-(trifluoromethyl)benzamido)-1*H*-benzo[*d*]imidazol-1-yl)propyl)carbamate (31b).** Yield, 68%. ^{1}H NMR (DMSO-d_6, 400 MHz): δ 12.7 (br s, 1H), 8.53 (d, J = 7.6 Hz, 1H), 8.46 (s, 1H), 7.88 (d, J = 8.0 Hz, 1H), 7.72 (d, J = 8.0 Hz, 1H), 7.41 (d, J = 8.4 Hz, 1H), 7.36 (s, 1H), 7.09 (d, J = 8.0 Hz, 1H), 6.85 (br s, 1H), 4.26 (t, J = 6.8 Hz, 2H), 3.29−2.98 (m, 2H), 2.40 (s, 3H), 1.92 (t, J = 7.2 Hz, 2H), 1.32 (s, 9H). MS calculated for $C_{24}H_{28}F_3N_4O_3$ $(M + H)^+$ 477.21, found 477.2.

***tert*-Butyl 3-(5-Methyl-2-(3-(trifluoromethyl)benzamido)-1*H*-benzo[*d*]imidazol-1-yl)azetidine-1-carboxylate (31c).** Yield, 60%.

***tert*-Butyl 3-(5-Methyl-2-(3-(trifluoromethyl)benzamido)-1*H*-benzo[*d*]imidazol-1-yl)pyrrolidine-1-carboxylate (31d).** Yield, 54%. ^{1}H NMR (DMSO-d_6, 400 MHz): δ 12.83 (s, 1H), 8.50 (d, J = 7.9 Hz, 1H), 8.45 (s, 1H), 7.95 (m, 1H), 7.72 (m, 1H), 7.42 (m, 1H), 7.41 (s, 1H), 7.09 (d, J = 7.8 Hz, 1H), 5.62 (m, 1H), 3.95 (m, 2H), 3.85 (m, 2H), 3.41 (m, 1H), 2.39 (s, 3H), 2.35 (m, 1H), 1.45 (s, 9H).

***tert*-Butyl 3-(5-Methyl-2-(3-(trifluoromethyl)benzamido)-1*H*-benzo[*d*]imidazol-1-yl)piperidine-1-carboxylate (31e).** Yield, 54%. ^{1}H NMR ($CDCl_3$, 400 MHz): δ 12.46 (s, 1H), 8.58 (s, 1H), 8.46 (d, J = 7.6 Hz, 1H), 7.73 (d, J = 7.6 Hz, 1H), 7.58−7.55 (m, 1H), 7.28 (s, 1H), 7.15 (s, 1H), 7.09 (d, J = 8.4 Hz, 1H), 4.60 (br s, 1H), 4.3 (br s, 2H), 3.79 (t, J = 8.0 Hz, 1H), 2.90−2.65 (m, 2H), 2.46 (s, 3H), 2.17−1.93 (m, 2H), 1.85−1.8 (m, 1H), 1.47 (s, 9H). MS calculated for $C_{26}H_{30}F_3N_4O_3$ $(M + H)^+$ 503.23, found 503.0.

***tert*-Butyl 4-(5-Methyl-2-(3-(trifluoromethyl)benzamido)-1*H*-benzo[*d*]imidazol-1-yl)piperidine-1-carboxylate (31f).** Yield, 66%. ^{1}H NMR (CD_3OD, 400 MHz): δ 8.50 (s, 1H), 8.47 (d, J = 7.5 Hz, 1H), 7.80 (d, J = 7.4 Hz, 1H), 7.62 (t, J = 7.5 Hz, 1H), 7.42 (d, J = 7.9 Hz, 1H), 7.35 (s, 1H), 7.36 (d, J = 7.5 Hz, 1H), 4.85−5.05 (m, 1H), 4.25−4.41 (m, 2H), 2.91−3.12 (m, 2H), 2.55−2.75 (m, 2H), 2.41 (s, 3H), 1.82−1.96 (m, 2H), 1.45 (s, 9H). MS calculated for $C_{26}H_{30}F_3N_4O_3$ $(M + H)^+$ 503.22, found 503.4.

***tert*-Butyl 3-(5-Methyl-2-(3-(trifluoromethyl)benzamido)-1*H*-benzo[*d*]imidazol-1-yl)azepane-1-carboxylate (31g).** Yield, 80%. MS calculated for $C_{27}H_{32}F_3N_4O_3$ $(M + H)^+$ 517.24, found 517.3.

***tert*-Butyl 4-(5-Methyl-2-(3-(trifluoromethyl)benzamido)-1*H*-benzo[*d*]imidazol-1-yl)azepane-1-carboxylate (31h).** Yield, 51%. ^{1}H NMR (DMSO-d_6, 400 MHz): δ 12.80 (d, J = 15.0 Hz, 1H), 8.51 (d, J = 6.8 Hz, 1H), 8.46 (s, 1H), 7.89 (d, J = 7.4 Hz, 1H), 7.61−7.81 (m, 1H), 7.54 (d, J = 8.3 Hz, 1H), 7.39 (s, 1H), 7.10 (d, J = 8.3 Hz, 1H), 4.65−5.01 (m, 1H), 3.15−4.05 (m, 4H), 2.49 (s, 3H), 1.65−2.15 (m, 6H), 1.21 and 1.41 (2s, 9H).

***tert*-Butyl (3-(5-Methyl-2-(3-(trifluoromethyl)benzamido)-1*H*-benzo[*d*]imidazol-1-yl)cyclopentyl)carbamate (31i).** Yield, 64%. ^{1}H NMR (DMSO-d_6, 400 MHz): δ 12.78 (s, 1H), 8.55 (d, J = 8.4 Hz, 1H), 8.43 (s, 1H), 7.88 (d, J = 7.6 Hz, 1H), 7.71 (d, J = 7.6 Hz, 1H), 7.53 (d, J = 8.0 Hz, 1H), 7.40 (s, 1H), 7.18−7.08 (m, 3H), 5.42 (t, J = 8.4 Hz, 1H), 4.01 (br s, 1H), 3.29 (s, 1H), 2.40−1.9 (m, 7H), 1.39 (s, 9H).

***tert*-Butyl (*cis*-2-(5-Methyl-2-(3-(trifluoromethyl)-benzamido)-1*H*-benzo[*d*]imidazol-1-yl)cyclohexyl)carbamate (31j).** Yield, 55%. ^{1}H NMR ($CDCl_3$, 400 MHz): δ 12.55 (br s, 1H), 8.56 (s, 1H), 8.43 (d, J = 7.3 Hz, 1H), 7.74 (d, J = 7.3 Hz, 1H), 7.58 (t, J = 7.9 Hz, 1H), 7.21 (m, 1H), 7.14 (s, 1H), 7.08 (d, J = 7.8 Hz, 1H), 4.55 (m, 1H), 4.21 (m, 1H), 3.15 (m, 1H), 2.44 (s, 3H), 1.45−2.15 (m, 8H), 1.06 (s, 9H). MS calculated for $C_{27}H_{32}F_3N_4O_3$ $(M + H)^+$ 517.23, found 517.3.

***tert*-Butyl (*trans*-2-(5-Methyl-2-(3-(trifluoromethyl)-benzamido)-1*H*-benzo[*d*]imidazol-1-yl)cyclohexyl)carbamate (31k).** Yield, 44%. ^{1}H NMR ($CDCl_3$, 400 MHz): δ 12.40 (s, 1H), 8.57 (s, 1H), 8.45 (d, J = 7.9 Hz, 1H), 7.74 (d, J = 7.3 Hz, 1H), 7.58 (t, J = 7.8 Hz, 1H), 7.36 (d, J = 7.4 Hz, 1H), 7.12 (s, 1H), 7.08 (d, J = 8.3 Hz, 1H), 4.11−4.95 (m, 3H), 2.44 (s, 3H), 1.85−2.35 (m, 4H), 1.31−1.55 (m, 4H), 1.15 (s, 9H). MS calculated for $C_{27}H_{32}F_3N_4O_3$ $(M + H)^+$ 517.23, found 517.4.

***tert*-Butyl (*cis*-3-(5-Methyl-2-(3-(trifluoromethyl)-benzamido)-1*H*-benzo[*d*]imidazol-1-yl)cyclohexyl)carbamate (31l).** Yield, 49%. ^{1}H NMR (DMSO-d_6, 400 MHz): δ 12.78 (s, 1H), 8.52 (d, J = 7.2 Hz, 1H), 8.46 (s, 1H), 7.89 (d, J = 7.2 Hz, 1H), 7.76−7.51 (m, 1H), 7.52 (d, J = 7.2 Hz, 1H), 7.38 (s, 1H), 7.08 (d, J = 8.4 Hz, 1H), 6.95 (d, J = 8.4 Hz, 1H), 4.91−4.75 (m, 1H), 3.62−3.41 (m, 1H), 2.39 (s, 3H), 2.35−2.24 (m, 2H), 1.99−1.75 (m, 4H), 1.35 (s, 9H), 1.59−1.29 (m, 2H). MS calculated for $C_{27}H_{32}F_3N_4O_3$ $(M + H)^+$ 517.24, found 517.3.

***tert*-Butyl (*trans*-3-(5-Methyl-2-(3-(trifluoromethyl)-benzamido)-1*H*-benzo[*d*]imidazol-1-yl)cyclohexyl)carbamate (31m).** Yield, 70%.

***tert*-Butyl (*cis*-4-(5-Methyl-2-(3-(trifluoromethyl)-benzamido)-1*H*-benzo[*d*]imidazol-1-yl)cyclohexyl)carbamate (31n).** Yield, 32%. ^{1}H NMR ($CDCl_3$, 400 MHz): δ 12.49 (s, 1H), 8.55 (s, 1H), 8.49 (d, J = 7.8 Hz, 1H), 7.73 (d, J = 7.3 Hz, 1H), 7.60 (d, J = 7.3 Hz, 1H), 7.29 (d, J = 8.3 Hz, 1H), 7.16 (s, 1H), 7.10 (d, J = 8.3 Hz, 1H), 4.61−4.85 (m, 2H), 3.81−3.99 (m, 1H), 2.41−2.59 (m, 2H), 2.42 (s, 3H), 2.01−2.19 (m, 2H), 1.65−1.95 (m, 4H), 1.41 (s, 9H). MS calculated for $C_{27}H_{32}F_3N_4O_3$ $(M + H)^+$ 517.23, found 517.1.

***tert*-Butyl (*trans*-4-(5-Methyl-2-(3-(trifluoromethyl)-benzamido)-1*H*-benzo[*d*]imidazol-1-yl)cyclohexyl)carbamate (31o).** Yield, 71%. ^{1}H NMR (DMSO-d_6, 400 MHz): δ 12.78 (s, 1H), 8.47 (s, 1H), 8.46 (s, 1H), 7.89 (d, J = 7.7 Hz, 1H), 7.74 (t, J = 8.2 Hz, 1H), 7.64 (d, J = 8.2 Hz, 1H), 7.39 (s, 1H), 7.06 (d, J = 7.2 Hz, 1H), 6.86 (d, J = 7.2 Hz, 1H),4.75 (m, 1H), 3.45 (m, 1H), 2.35 (s, 3H), 1.75−2.05 (m, 4H), 1.45 (s, 9H), 1.3−1.51 (m, 4H). MS calculated for $C_{27}H_{32}F_3N_4O_3$ $(M + H)^+$ 517.23, found 517.2.

***tert*-Butyl (2-(5-Methyl-2-(3-(trifluoromethyl)benzamido)-1*H*-benzo[*d*]imidazol-1-yl)phenyl)carbamate (31p).** Yield, 71%. ^{1}H NMR (DMSO-d_6, 400 MHz): δ 12.93 (s, 1H), 8.98 (s, 1H), 8.26 (s, 1H), 8.24 (d, J = 7.8 Hz, 1H), 7.86 and 7.81 (2d, J = 7.8 Hz, 2H), 7.63 (t, J = 7.8 Hz, 1H), 7.53 (m, 2H), 7.43 (s, 1H), 7.31 (m, 1H), 7.01 (d, J = 8.3 Hz, 1H), 6.79 (d, J = 8.3 Hz, 1H), 2.41 (s, 3H), 1.24 (s, 9H). MS calculated for $C_{27}H_{26}F_3N_4O_3$ $(M + H)^+$ 511.19, found 511.1.

***tert*-Butyl (3-(5-Methyl-2-(3-(trifluoromethyl)benzamido)-1*H*-benzo[*d*]imidazol-1-yl)phenyl)carbamate (31q).** Yield, 76%. MS calculated for $C_{27}H_{26}F_3N_4O_3$ $(M + H)^+$ 511.20, found 511.1.

***tert*-Butyl Methyl(3-(5-methyl-2-(3-(trifluoromethyl)-benzamido)-1*H*-benzo[*d*]imidazol-1-yl)phenyl)carbamate (31r).** Yield, 67%. ^{1}H NMR (DMSO-d_6, 400 MHz): δ 12.99 (s, 1H), 8.32 (d, J = 6.8 Hz, 2H), 7.84 (d, J = 7.2 Hz, 1H), 7.67−7.45 9 (m, 6H), 7.14 (d, J = 8.0 Hz, 1H), 7.08 (d, J = 8.0 Hz, 1H), 3.28 (s, 3H), 2.42 (s, 3H), 1.41 (s, 9H). MS calculated for $C_{28}H_{28}F_3N_4O_3$ $(M + H)^+$ 525.21, found 524.9.

***tert*-Butyl (3-(5-Methyl-2-(3-(trifluoromethyl)benzamido)-1*H*-benzo[*d*]imidazol-1-yl)phenyl)carbamate (31s).** Yield, 60%. ^{1}H NMR (DMSO-d_6, 400 MHz): δ 12.94 (s, 1H), 9.67 (s, 1H), 8.32 (s, 1H), 8.28 (d, J = 7.8 Hz, 1H), 7.84 (d, J = 7.3 Hz, 1H), 7.45−7.75

DOI: 10.1021/acs.jmedchem.5b01985
J. Med. Chem. 2016, 59, 6671−6689

(m, 6H), 7.24 (s, 1H), 7.03 (s, 1H), 2.41 (s, 3H), 1.52 (s, 9H). MS calculated for $C_{27}H_{26}F_3N_4O_3$ (M + H)$^+$ 511.19, found 511.3.

***tert*-Butyl (*R*)-3-(7-Methyl-2-(3-(trifluoromethyl)benzamido)-1*H*-benzo[*d*]imidazol-1-yl)azepane-1-carboxylate (39).** ^{1}H NMR (DMSO-d_6, 500 MHz) δ 12.94 (s, 1H), 8.59−8.47 (m, 1H), 8.43 (t, J = 6.7 Hz, 1H), 7.91 (d, J = 7.6 Hz, 1H), 7.84−7.67 (m, 1H), 7.46 (d, J = 7.7 Hz, 1H), 7.13 (t, J = 7.7 Hz, 1H), 7.09−6.97 (m, 1H), 4.96−4.72 (m, 1H), 4.50−4.21 (m, 1H), 3.86 (d, J = 12.6 Hz, 1H), 3.83−3.73 (m, 1H), 3.26−3.13 (m, 1H), 2.83−2.74 (m, 1H), 2.71 (s, 3H), 2.07 (m, 2H), 1.96 (m, 1H), 1.78 (m, 1H), 1.45 (s, 9H), 1.23 (m, 1H). MS calculated for $C_{27}H_{32}F_3N_4O_3$ (M + H)$^+$ 517.24, found 517.4. $[\alpha]_D^{23}$ +121.95° (c 0.123, MeOH).

***tert*-Butyl (*R*)-3-(7-Methyl-2-(2-(trifluoromethyl)-isonicotinamido)-1*H*-benzo[*d*]imidazol-1-yl)azepane-1-carboxylate (40).** Yield, 63%. ^{1}H NMR ($CDCl_3$, 400 MHz) δ 12.53 (s, 1H), 8.89 (d, J = 4.6 Hz, 1H), 8.54 (d, J = 7.1 Hz, 1H), 8.27 (d, J = 4.6 Hz, 1H), 7.21 (dt, J = 7.8, 21.3 Hz, 2H), 7.08 (t, J = 9.2 Hz, 1H), 5.12−4.85 (m, 1H), 4.34 (dd, J = 10.6, 13.6 Hz, 1H), 4.16−3.85 (m, 2H), 3.36−3.21 (m, 1H), 2.94−2.82 (m, 1H), 2.80 (s, 3H), 2.30−2.15 (m, 1H), 2.15−2.00 (m, 2H), 2.00−1.81 (m, 1H), 1.48 (s, 9H), 1.43−1.36 (m, 1H). MS calculated for $C_{26}H_{31}F_3N_5O_3$ (M + H)$^+$ 518.23, found 518.2. $[\alpha]_D^{23}$ +99.60° (c 0.251, MeOH).

***tert*-Butyl (*R*)-3-(7-Methyl-2-(2-methylisonicotinamido)-1*H*-benzo[*d*]imidazol-1-yl)azepane-1-carboxylate (41).** Yield, 100%. ^{1}H NMR (DMSO-d6, 400 MHz) δ 12.95 (s, 1H), 8.60 (t, J = 4.6 Hz, 1H), 7.89 (d, J = 5.7 Hz, 1H), 7.81 (t, J = 4.9 Hz, 1H), 7.46 (d, J = 7.2 Hz, 1H), 7.14 (t, J = 7.7 Hz, 1H), 7.10−7.02 (m, 1H), 4.96−4.71 (m, 1H), 4.32 (dd, J = 10.5, 13.4 Hz, 1H), 3.88−3.78 (m, 1H), 3.78−3.65 (m, 1H), 3.29−3.17 (m, 1H), 2.83−2.74 (m, 1H), 2.71 (s, 3H), 2.57 (s, 3H), 2.14−2.02 (m, 2H), 2.02−1.91 (m, 1H), 1.89−1.71 (m, 1H), 1.45 (s, 9H), 1.39−1.33 (m, 1H); MS calculated for $C_{26}H_{34}N_5O_3$ (M + H)$^+$ 464.26, found 464.2. $[\alpha]_D^{23}$ +35.46° (c 0.282, MeOH).

***tert*-Butyl (*R*)-3-(7-Chloro-2-(2-methylisonicotinamido)-1*H*-benzo[*d*]imidazol-1-yl)azepane-1-carboxylate (42).** Yield, 100%. ^{1}H NMR ($CDCl_3$, 400 MHz): δ 12.81 (br s, 1H), 8.65−8.62 (m, 1H), 7.95−7.85 (m, 2H), 7.27−7.11 (m, 3H), 5.64−5.51 (m, 1H), 4.56−4.44 (m, 1H), 4.07−3.92 (m, 1H), 3.79−3.71 (m, 0.5H), 3.41−3.35 (m, 0.5H), 3.29−3.23 (m, 1H), 2.71−2.59 (m, 1H), 2.65 (s, 3H), 2.22−2.00 (m, 3H), 1.93−1.80 (m, 1H), 1.51−1.45 (m, 1H), 1.50 (s, 3.5H), 1.41 (s, 5.5H). MS calculated for $C_{25}H_{31}ClN_5O_3$ (M + H)$^+$ 484.20, found 484.20. $[\alpha]_D^{23}$ +89.29° (c 0.112, MeOH).

General Procedure for the Synthesis of Compounds 32a−s and 43. Synthesis of *N*-(1-(1-Acryloylpiperidin-3-yl)-5-methyl-1*H*-benzo[*d*]imidazol-2-yl)-3-(trifluoromethyl)benzamide (32e). To a stirred solution of **31e** (0.300 g, 0.59 mmol) in CH_2Cl_2 (25 mL) at room temperature was added TFA (0.170 g, 1.49 mmol), and the reaction mixture was stirred for 2 h, and then the volatiles were removed under reduced pressure. The residue was then partitioned between saturated aqueous $NaHCO_3$ (15 mL) and CH_2Cl_2 (20 mL), and the aqueous layer was extracted once more with CH_2Cl_2 (20 mL). The pooled organic extracts were washed with brine, dried over anhydrous Na_2SO_4, filtered, and concentrated under reduced pressure to afford (*S*)-*N*-(5-methyl-1-(piperidin-3-yl)-1*H*-benzo[*d*]imidazol-2-yl)-3-(trifluoromethyl)benzamide (0.200 g, 83%), which was used as is without further purification. To a 0 °C solution of (*S*)-*N*-(5-methyl-1-(piperidin-3-yl)-1*H*-benzo[*d*]imidazol-2-yl)-3-(trifluoromethyl)-benzamide (0.150 g, 0.37 mmol) in CH_2Cl_2 (20 mL) was added acryloyl chloride (0.050 g, 0.55 mmol), and the reaction mixture was stirred for 30 min at 0 °C. The reaction mixture was partitioned between water (10 mL) and CH_2Cl_2 (10 mL), and the layers were separated. The aqueous layer was extracted with CH_2Cl_2 (2 × 20 mL), and the combined organic layers were washed with brine, dried over anhydrous Na_2SO_4, filtered, concentrated under reduced pressure, and the resulting residue was purified by column chromatography (50% EtOAc/hexane gradient) to give **32e** (0.120 g, 0.329 mmol, 70%). ^{1}H NMR (DMSO-d_6, 400 MHz): δ 12.84 (s, 1H), 8.46 (d, J = 8.0 Hz, 2H), 7.89 (d, J = 8.0 Hz, 1H), 7.75−7.63 (m, 2H), 7.39 (s, 1H), 7.09 (d, J = 8.4 Hz, 1H), 6.95−6.79 (m, 1H), 6.19−6.13 (m, 1H), 5.75−5.59 (m, 1H), 4.79−4.56 (m, 2H), 4.31−4.19 (m, 1H), 4.15−3.65 (m, 1H), 3.27−2.66 (m, 2H), 2.39 (s, 3H), 2.00−1.91 (m, 2H), 1.64−1.5 (m, 1H); MS calculated for $C_{24}H_{24}F_3N_4O_2$ (M + H)$^+$ 457.19, found 456.9.

***N*-(1-(2-Acrylamidoethyl)-5-methyl-1*H*-benzo[*d*]imidazol-2-yl)-3-(trifluoromethyl)benzamide (32a).** Yield, 45%. ^{1}H NMR (DMSO-d_6, 400 MHz): δ 12.73 (s, 1H), 8.53 (d, J = 8.0 Hz, 1H), 8.47 (s, 1H), 8.26−8.23 (m, 1H), 7.88 (d, J = 8.0 Hz, 1H), 7.70 (t, J = 8.0 Hz, 1H), 7.38−7.32 (m, 2H), 7.08 (d, J = 7.8 Hz, 1H), 6.97 (d, J = 7.6 Hz, 2H), 5.43 (7, J = 8.0 Hz, 1H), 4.40−4.37 (m, 2H), 3.59−3.56 (m, 2H), 2.40 (s, 3H). MS calculated for $C_{21}H_{20}F_3N_4O_2$ (M + H)$^+$ 417.15, found 416.8.

***N*-(1-(3-Acrylamidopropyl)-5-methyl-1*H*-benzo[*d*]imidazol-2-yl)-3-(trifluoromethyl)benzamide (32b).** Yield, 35%. ^{1}H NMR (DMSO-d_6, 400 MHz): δ 12.74 (s, 1H), 8.51 (d, J = 8.0 Hz, 1H), 8.45 (s, 1H), 8.21 (d, J = 5.6 Hz, 1H), 7.88 (d, J = 7.6 Hz, 1H), 7.72−7.68 (m, 1H), 7.44 (d, J = 8.0 Hz, 1H), 7.37 (m, 1H), 7.10 (d, J = 7.2 Hz, 1H), 6.23−6.02 (m, 2H), 5.56 (d, J = 2.0, 8.0 Hz, 1H), 4.32−4.28 (m, 2H), 3.33 (s, 1H), 3.25−3.20 (m, 1H), 2.40 (s, 3H), 1.99−1.94 (m, 2H). MS calculated for $C_{22}H_{22}F_3N_4O_2$ (M + H)$^+$ 431.17, found 431.1.

***N*-(1-(1-Acryloylazetidin-3-yl)-5-methyl-1*H*-benzo[*d*]-imidazol-2-yl)-3-(trifluoromethyl)benzamide (32c).** Yield, 58%. ^{1}H NMR (DMSO-d_6, 400 MHz): δ 12.86 (s, 1H), 8.46−8.42 (m, 2H), 7.87 (d, J = 7.8 Hz, 1H), 7.63 (t, J = 7.8 Hz, 1H), 7.43 (d, J = 8.4 Hz, 1H), 7.40 (s, 1H), 7.13 (d, J = 7.8 Hz, 1H), 6.45 (dd, J = 10.2, 16.6 Hz, 1H), 6.24 (dd, J = 1.9, 17.1 Hz, 1H), 5.86−5.74 (m, 2H), 5.03−5.0 (m, 1H), 4.77−4.68 (m, 2H), 4.46 (t, J = 9.7 Hz, 1H), 2.40 (s, 3H). MS calculated for $C_{22}H_{20}F_3N_4O_2$ (M + H)$^+$ 429.15, found 429.0.

***N*-(1-(1-Acryloylpyrrolidin-3-yl)-5-methyl-1*H*-benzo[*d*]-imidazol-2-yl)-3-(trifluoromethyl)benzamide (32d).** Yield, 28%. ^{1}H NMR (DMSO-d_6, 400 MHz): δ 12.83 (s, 1H), 8.51−8.48 (m, 1H), 8.42 (s, 1H), 7.88 (d, J = 8.0 Hz, 1H), 7.69−7.64 (m, 1H), 7.48−7.39 (m, 2H), 7.10 (d, J = 8.4 Hz, 1H), 6.78−6.54 (m, 1H), 6.26−6.17 (m, 1H), 5.78−5.60 (m, 2H), 4.27−4.22 (m, 0.5H), 4.13−4.00 (m, 1.5H), 3.95−3.86 (m, 1H), 3.79−3.73 (m, 0.5H), 3.58−3.51 (m, 0.5H), 2.83−2.71 (m, 1H), 2.40 (s, 3H), 2.38−2.25 (m, 1H). MS calculated for $C_{23}H_{22}F_3N_4O_2$ (M + H)$^+$ 443.13, found 442.8.

***N*-(1-(1-Acryloylpiperidin-4-yl)-5-methyl-1*H*-benzo[*d*]-imidazol-2-yl)-3-(trifluoromethyl)benzamide (32f).** Yield, 41%. ^{1}H NMR (DMSO-d_6, 400 MHz): δ 12.79 (s, 1H), 8.46−8.40 (m, 2H), 7.88 (d, J = 8.0 Hz, 1H), 7.70−7.63 (m, 1H), 7.51 (d, J = 8.4 Hz, 1H), 7.38 (s, 1H), 7.07 (d, J = 8.4 Hz, 1H), 6.96−6.89 (m, 1H), 6.22−6.18 (m, 1H), 5.75−5.69 (m, 1H), 5.04−4.97 (m, 1H), 4.73−4.65 (m, 1H), 4.34−4.29 (m, 1H), 3.30−3.28 (m, 1H), 2.87−2.81 (m, 1H), 2.68−2.54 (m, 2H), 2.40 (s, 3H), 2.00−1.93 (m, 2H). MS calculated for $C_{24}H_{24}F_3N_4O_2$ (M + H)$^+$ 457.19, found 457.3.

***N*-(1-(1-Acryloylazepan-3-yl)-5-methyl-1*H*-benzo[*d*]-imidazol-2-yl)-3-(trifluoromethyl)benzamide (32g).** Yield, 38%. ^{1}H NMR (DMSO-d_6, 400 MHz): δ 12.81 (d, J = 19.6 Hz, 1H), 8.54 (s, 1H), 8.48−8.44 (m, 1H), 7.90−7.51 (m, 3H), 7.39 (d, J = 4.8 Hz, 1H), 7.10 (d, J = 7.6 Hz, 1H), 6.87−6.81 (m, 1H), 6.25−6.17 (m, 1H), 5.76−5.50 (m, 1H), 4.88 (br s, 1H), 4.16−4.03 (m, 2H), 3.90−3.63 (m, 1H), 3.37−3.22 (m, 1H), 2.40 (s, 4H), 2.05−1.85 (m, 4H), 1.43−1.40 (m, 1H). MS calculated for $C_{25}H_{26}F_3N_4O_2$ (M + H)$^+$ 471.20, found 471.2.

***N*-(1-(1-Acryloylazepan-4-yl)-5-methyl-1*H*-benzo[*d*]-imidazol-2-yl)-3-(trifluoromethyl)benzamide (32h).** Yield, 41%. ^{1}H NMR (DMSO-d_6, 400 MHz): δ 12.74 (s, 1H), 8.45−8.37 (m, 2H), 7.87 (d, J = 7.4 Hz, 1H), 7.67 (t, J = 7.8 Hz, 1H), 7.50 (d, J = 8.3 Hz, 1H), 7.38 (s, 1H), 7.08 (d, J = 8.3 Hz, 1H), 6.92−6.81 (m, 1H), 6.29−6.24 (m, 1H), 5.78−5.67 (m, 1H), 4.90 (br s, 1H), 3.92−3.43 (m, 4H), 2.60−2.56 (m, 1H), 2.39 (s, 3H), 2.10−1.78 (m, 4H), 1.25−1.21 (m, 1H). MS calculated for $C_{25}H_{26}F_3N_4O_2$ (M + H)$^+$ 471.20, found 471.0.

***N*-(1-(3-Acrylamidocyclopentyl)-5-methyl-1*H*-benzo[*d*]-imidazol-2-yl)-3-(trifluoromethyl)benzamide (32i).** Yield, 17%. ^{1}H NMR (DMSO-d_6, 400 MHz): δ 12.78 (s, 1H), 8.55 (d, J = 8.0 Hz, 1H), 8.45 (s, 1H), 8.40 (d, J = 7.2 Hz, 1H), 7.89 (d, J = 8.0 Hz, 1H), 7.75−7.73 (m, 1H), 7.50 (d, J = 7.6 Hz, 1H), 7.40 (s, 1H), 7.10 (d, J = 7.6 Hz, 1H), 6.27−6.20 (m, 1H), 6.11 (dd, J = 2.0, 14.4 Hz, 1H), 5.61 (d, J = 2.0 Hz, 1H), 5.59−5.42 (m, 1H), 4.35−4.29 (m, 1H),

DOI: 10.1021/acs.jmedchem.5b01985
J. Med. Chem. 2016, 59, 6671−6689

2.40 (s, 3H), 2.37−1.92 (m, 6H). MS calculated for $C_{24}H_{24}F_3N_4O_2$ $(M + H)^+$ 457.19, found 457.40.

***N*-(1-(*cis*-2-Acrylamidocyclohexyl)-5-methyl-1*H*-benzo[*d*]-imidazol-2-yl)-3-(trifluoromethyl)benzamide (32j).** Yield, 45%. ^{1}H NMR ($CDCl_3$, 400 MHz): δ 12.61 (s, 1H), 8.91 (s, 1H), 8.55 (s, 1H), 8.41 (d, J = 7.9 Hz, 1H), 7.79 (d, J = 5.8 Hz, 1H), 7.66−7.62 (m, 1H), 7.19−7.11 (m, 3H), 6.0 (d, J = 16.7 Hz, 1H), 5.60−5.52 (m, 1H), 5.20 (d, J = 10.2 Hz, 1H), 4.46−4.44 (m, 2H), 3.50−3.41 (m, 1H), 2.53−2.46 (m, 1H), 2.45 (s, 3H), 2.13−2.10 (m, 1H), 1.98−1.94 (m, 1H), 1.69−1.56 (m, 3H), 1.55−1.43 (m, 1H). MS calculated for $C_{25}H_{26}F_3N_4O_2$ $(M + H)^+$ 471.20, found 471.8.

***N*-(1-(*trans*-2-Acrylamidocyclohexyl)-5-methyl-1*H*-benzo[*d*]-imidazol-2-yl)-3-(trifluoromethyl)benzamide (32k).** Yield, 45%. ^{1}H NMR ($CDCl_3$, 400 MHz): δ 12.32 (s, 1H), 8.57 (s, 1H), 8.47 (d, J = 7.3 Hz, 1H), 7.77 (d, J = 7.9 Hz, 1H), 7.62−7.58 (m, 1H), 7.42−7.40 (m, 1H), 7.12−7.06 (m, 2H), 6.18 (br s, 1H), 5.91 (dd, J = 1.5, 17.1 Hz, 1H), 5.73−5.67 (m, 1H), 5.36 (dd, J = 1.5, 10.3 Hz, 1H), 5.01−4.96 (m, 1H), 4.56 (br s, 1H), 2.43−2.38 (m, 4H), 2.12−1.94 (m, 3H), 1.56−1.42 (m, 4H). MS calculated for $C_{25}H_{26}F_3N_4O_2$ $(M + H)^+$ 471.20, found 471.2.

***N*-(1-(*cis*-3-Acrylamidocyclohexyl)-5-methyl-1*H*-benzo[*d*]-imidazol-2-yl)-3-(trifluoromethyl)benzamide (32l).** Yield, 26%. ^{1}H NMR (DMSO-d_6, 400 MHz): δ 12.79 (s, 1H), 8.52 (d, J = 8.0 Hz, 1H), 8.49 (s, 1H), 8.15 (d, J = 7.6 Hz, 1H), 7.90 (d, J = 8.0 Hz, 1H), 7.76 (d, J = 8.0 Hz, 1H), 7.57 (d, J = 8.4 Hz, 1H), 7.38 (s, 1H), 7.09 (d, J = 8.4 Hz, 1H), 6.22−6.08 (m, 1H), 6.04 (d, J = 2.0 Hz, 1H), 5.55 (dd, J = 2.4, 8.0 Hz, 1H), 4.98−4.77 (m, 1H), 3.99−3.83 (m, 1H), 2.41 (s, 3H), 2.50−2.35 (m, 2H), 1.96−1.80 (m, 4H), 1.62−1.30 (m, 2H). MS calculated for $C_{25}H_{26}F_3N_4O_2$ $(M + H)^+$ 471.20, found 471.2.

***N*-(1-(*trans*-3-Acrylamidocyclohexyl)-5-methyl-1*H*-benzo[*d*]-imidazol-2-yl)-3-(trifluoromethyl)benzamide (32m).** Yield, 20%. ^{1}H NMR ($CDCl_3$, 400 MHz): δ 12.39 (s, 1H), 8.55 (s, 1H), 8.40 (d, J = 7.6 Hz, 1H), 7.72 (d, J = 8.0 Hz, 1H), 7.54 (t, J = 7.6 Hz, 1H), 7.30−7.28 (m, 1H), 7.14 (s, 1H), 7.06 (d, J = 8.4 Hz, 1H), 6.99−6.20 (m, 2H), 5.88 (br s, 1H), 5.71 (d, J = 10.4 Hz, 1H), 5.06 (t, J = 12.8 Hz, 1H), 4.56 (br s, 1H), 2.55 (t, J = 12.4 Hz, 1H), 2.44−2.22 (m, 5H), 2.03−2.01 (m, 3H), 1.76−1.41 (m, 2H). MS calculated for $C_{25}H_{26}F_3N_4O_2$ $(M + H)^+$ 471.20, found 471.2.

***N*-(1-(*cis*-4-Acrylamidocyclohexyl)-5-methyl-1*H*-benzo[*d*]-imidazol-2-yl)-3-(trifluoromethyl)benzamide (32n).** Yield, 30%. ^{1}H NMR (DMSO-d_6, 400 MHz): δ 12.80 (s, 1H), 8.56 (d, J = 7.8 Hz, 1H), 8.43 (s, 1H), 8.27 (d, J = 5.9 Hz, 1H), 7.89 (d, J = 7.8 Hz, 1H), 7.73−7.64 (m, 2H), 7.40 (s, 1H), 7.11 (d, J = 8.1 Hz, 1H), 6.58−6.51 (m, 1H), 6.18−6.13 (m, 1H), 5.67−5.64 (m, 1H), 4.98−4.89 (m, 1H), 4.05 (br s, 1H), 3.34−3.28 (m, 2H), 2.40 (s, 3H), 2.06−2.02 (m, 2H), 1.83−1.68 (m, 4H). MS calculated for $C_{25}H_{26}F_3N_4O_2$ $(M + H)^+$ 471.20, found 471.0.

***N*-(1-(*trans*-4-Acrylamidocyclohexyl)-5-methyl-1*H*-benzo[*d*]-imidazol-2-yl)-3-(trifluoromethyl)benzamide (32o).** Yield, 44%. ^{1}H NMR (DMSO-d_6, 400 MHz): δ 12.80 (s, 1H), 8.46 (m, 2H), 8.10 (d, J = 7.8 Hz, 1H), 7.90 (d, J = 7.8 Hz, 1H), 7.78−7.65 (m, 2H), 7.40 (s, 1H), 7.10 (d, J = 8.0 Hz, 1H), 6.28−6.21 (m, 1H), 6.16−6.11 (m, 1H), 5.61−5.58 (m, 1H), 4.87−4.81 (m, 1H), 3.98−3.89 (m, 1H), 3.34−3.28 (m, 2H), 2.40 (s, 3H), 2.08−2.02 (m, 2H), 1.90−1.82 (m, 2H), 1.57−1.43 (m, 2H). MS calculated for $C_{25}H_{26}F_3N_4O_2$ $(M + H)^+$ 471.20, found 471.0.

***N*-(1-(2-Acrylamidophenyl)-5-methyl-1*H*-benzo[*d*]imidazol-2-yl)-3-(trifluoromethyl)benzamide (32p).** Yield, 24%. ^{1}H NMR (DMSO-d_6, 400 MHz): δ 12.94 (s, 1H), 9.61 (s, 1H), 8.25−8.22 (m, 2H), 8.15 (d, J = 7.8 Hz, 1H), 7.81 (d, J = 7.8 Hz, 2H), 7.64−7.54 (m, 2H), 7.43 (s, 1H), 7.39−7.35 (m, 1H), 6.99 (d, J = 7.3 Hz, 1H), 6.72 (d, J = 7.8 Hz, 1H), 6.23−6.16 (m, 1H), 6.10−6.05 (m, 1H), 5.56−5.52 (m, 1H), 2.40 (s, 3H). MS calculated for $C_{25}H_{20}F_3N_4O_2$ $(M + H)^+$ 465.15, found 465.1.

***N*-(1-(3-Acrylamidophenyl)-5-methyl-1*H*-benzo[*d*]imidazol-2-yl)-3-(trifluoromethyl)benzamide (32q).** Yield, 35%. ^{1}H NMR (DMSO-d_6, 400 MHz): δ 12.99 (s, 1H), 10.44 (s, 1H), 8.36 (s, 1H), 8.32 (d, J = 7.6 Hz, 1H), 8.19 (s, 1H), 7.83 (d, J = 7.6 Hz, 1H), 7.75 (d, J = 8.0 Hz, 1H), 7.67−7.58 (m, 2H), 7.46−7.41 (m, 2H), 7.20−7.09 (m, 2H), 6.49−6.30 (m, 1H), 6.29−6.25 (m, 1H), 5.80−5.75 (m, 1H), 2.42 (s, 3H). MS calculated for $C_{25}H_{20}F_3N_4O_2$ $(M + H)^+$ 465.15, found 465.2.

***N*-(5-Methyl-1-(3-(*N*-methylacrylamido)phenyl)-1*H*-benzo-[*d*]imidazol-2-yl)-3-(trifluoromethyl)benzamide (32r).** Yield, 44%. ^{1}H NMR (DMSO-d_6, 400 MHz): δ 13.01 (s, 1H), 8.30 (d, J = 6.4 Hz, 2H), 7.84 (d, J = 7.6 Hz, 1H), 7.75−7.62 (m, 4H), 7.50 (d, J = 1.6 Hz, 1H), 7.49−7.45 (m, 1H), 7.17−7.08 (m, 2H), 6.27−6.16 (m, 2H), 5.58−5.55 (m, 1H), 3.34 (s, 3H), 2.42 (s, 3H). MS calculated for $C_{26}H_{22}F_3N_4O_2$ $(M + H)^+$ 479.17, found 478.7.

***N*-(1-(4-Acrylamidophenyl)-5-methyl-1*H*-benzo[*d*]imidazol-2-yl)-3-(trifluoromethyl)benzamide (32s).** Yield, 48%. ^{1}H NMR (DMSO-d_6, 400 MHz): δ 12.99 (s, 1H), 10.43 (s, 1H), 8.38 (s, 1H), 8.32 (d, J = 7.6 Hz, 1H), 7.97 (d, J = 7.6 Hz, 2H), 7.83 (d, J = 7.6 Hz, 1H), 7.67−7.58 (m, 2H), 7.42 (m, 2H), 7.12−7.05 (m, 2H), 6.56−6.48 (m, 1H), 6.35−6.32 (m, 1H), 5.82−5.80 (m, 1H), 2.42 (s, 3H). MS calculated for $C_{25}H_{20}F_3N_4O_2$ $(M + H)^+$ 465.15, found 465.3.

***(R)*-*N*-(1-(1-Acryloylazepan-3-yl)-7-methyl-1*H*-benzo[*d*]-imidazol-2-yl)-3-(trifluoromethyl)benzamide (43).** Yield, 71%. ^{1}H NMR (DMSO-d_6, 400 MHz): δ 12.80 (br s, 1H), 8.52 (s, 1H), 8.42 (d, J = 8.0 Hz, 1H), 7.85−7.70 (m, 2H), 7.46 (d, J = 8.0 Hz, 1H), 7.13 (d, J = 8.0 Hz, 1H), 7.02 (d, J = 7.6 Hz, 1H), 6.82−6.75 (m, 1H), 6.15 (dd, J = 2.4, 14.0 Hz, 1H), 5.66 (br s, 1H), 5.0 (br s, 1H), 4.25−4.22 (m, 2H), 4.0 (br s, 1H), 3.50 (br s, 1H), 2.7−2.65 (m, 4H), 2.10−1.89 (m, 4H), 1.42−1.39 (m, 1H). MS calculated for $C_{25}H_{26}F_3N_4O_2$ $(M + H)^+$ 471.20, found 471.3. $[\alpha]_D^{23}$ +127.2° (c 0.0786, MeOH).

General Procedure for the Synthesis of Compounds 44−46. Synthesis of (*R*,*E*)-*N*-(1-(1-(4-(Dimethylamino)but-2-enoyl)-azepan-3-yl)-7-methyl-1*H*-benzo[*d*]imidazol-2-yl)-2-methyl-isonicotinamide (46). A solution of **41** (6.81 g, 14.7 mmol) in MeOH (15 mL) was treated with 4 M HCl in dioxane (100 mL, 400 mmol) and stirred for 12 h. The volatiles were removed under reduced pressure to afford (*R*)-*N*-(1-(azepan-3-yl)-7-methyl-1*H*-benzo[*d*]imidazol-2-yl)-2-methylisonicotinamide, which was dissolved in CH_2Cl_2 (70 mL) and Et_3N (6.15 mL, 44.1 mmol). In a separate flask, a mixture of (*E*)-4-(dimethylamino)but-2-enoic acid hydrochloride (2.60 g, 19.1 mmol) and HATU (7.34 g, 19.1 mmol) in CH_2Cl_2 (50 mL) was treated with Et_3N (3.07 mL, 22.0 mmol) and stirred at room temperature for 30 min. This was then treated with the CH_2Cl_2/Et_3N solution of (*R*)-*N*-(1-(azepan-3-yl)-7-methyl-1*H*-benzo[*d*]imidazol-2-yl)-2-methylisonicotinamide, and the transfer was assisted with an additional volume of CH_2Cl_2 (20 mL). The reaction mixture was stirred for 30 min and then washed with 1 M NaOH (100 mL). The aqueous layer was extracted with CH_2Cl_2 (2 × 150 mL), and the pooled organics were washed with 1 M NaOH (100 mL) and then brine (100 mL), dried over Na_2SO_4, filtered, and concentrated under reduced pressure. The crude material was purified by column chromatography (0−70% (9:1:0.175N CH_2Cl_2/MeOH/NH_3)/CH_2Cl_2 gradient) to afford **46** (4.26 g, 61%). ^{1}H NMR (CD_3OD, 400 MHz) δ 8.57 (d, J = 5.2 Hz, 1H), 8.06 (s, 1H), 7.98 (d, J = 5.2 Hz, 1H), 7.40 (d, J = 8.2 Hz, 1H), 7.19 (t, J = 7.8 Hz, 1H), 7.10 (t, J = 8.7 Hz, 1H), 6.99 (t, J = 15.8 Hz, 1H), 6.75 (m, 1H), 5.14 (m, 2H), 4.60 (m, 1H), 4.32 (d, J = 13.0 Hz, 1H), 3.98 (m, 3H), 3.71 (m, 1H), 3.16 (m, 1H), 3.03 (m, 1H), 2.93 (s, 6H), 2.77 (s, 3H), 2.53 (s, 3H), 2.22 (m, 1H), 2.12 (m, 2H). MS calculated for $C_{27}H_{35}N_6O_2$ $(M + H)^+$ 475.28, found 475.1. $[\alpha]_D^{23}$ +72.46° (c 0.069, MeOH).

***(R,E)*-*N*-(1-(1-(4-(Dimethylamino)but-2-enoyl)azepan-3-yl)-7-methyl-1*H*-benzo[*d*]imidazol-2-yl)-3-(trifluoromethyl)-benzamide (44).** Yield, 55%. ^{1}H NMR ($CDCl_3$, 400 MHz) δ 12.61 (s, 1H), 8.66 (s, 1H), 8.44 (d, J = 7.6 Hz, 1H), 7.77 (d, J = 7.2 Hz, 1H), 7.62 (t, J = 7.7 Hz, 1H), 7.18 (m, 2H), 7.03 (m, 1H), 6.92 (dt, J = 6.1, 15.2 Hz, 1H), 6.59 (d, J = 15.2 Hz, 1H), 5.10 (m, 1H), 4.46 (m, 2H), 4.01 (dt, J = 7.3, 14.4 Hz, 1H), 3.66 (m, 1H), 3.25 (s, 2H), 2.97 (s, 1H), 2.80 (s, 3H), 2.41 (s, 6H), 2.08 (m, 3H), 1.58 (m, 2H). MS calculated for $C_{28}H_{33}F_3N_5O_2$ $(M + H)^+$ 528.26, found 528.2. $[\alpha]_D^{23}$ +106.38° (c 0.141, MeOH).

***(R,E)*-*N*-(1-(1-(4-(Dimethylamino)but-2-enoyl)azepan-3-yl)-7-methyl-1*H*-benzo[*d*]imidazol-2-yl)-2-(trifluoromethyl)-isonicotinamide (45).** Yield, 55%. ^{1}H NMR (CD_3OD, 400 MHz) δ 8.88 (d, J = 4.9 Hz, 1H), 8.56 (s, 1H), 8.34 (d, J = 4.9 Hz, 1H), 7.41 (d, J = 8.0 Hz, 1H), 7.20 (t, J = 7.8 Hz, 1H), 7.12 (m, 1H),

DOI: 10.1021/acs.jmedchem.5b01985
J. Med. Chem. 2016, 59, 6671−6689

6.86 (t, J = 13.8 Hz, 1H), 6.78 (m, 1H), 5.12 (m, 1H), 4.54 (dd, J = 10.8, 13.0 Hz, 1H), 4.27 (m, 1H), 4.02 (m, 1H), 3.65 (m, 3H), 2.92 (m, 1H), 2.78 (s, 3H), 2.67 (s, 6H), 2.22 (m, 1H), 2.08 (m, 3H), 1.49 (m, 1H). MS calculated for $C_{27}H_{32}F_3N_6O_2$ $(M + H)^+$ 529.25, found 529.2. Anal. Calcd for $C_{27}H_{31}F_3N_6O_2$ (528.58): C 61.35, H 5.91, N 15.90. Found: C 61.10, H 5.93, N 15.75. $[\alpha]_D^{23}$ +153.06° (c 0.098, MeOH).

Synthesis of (*R*,*E*)-*N*-(7-Chloro-1-(1-(4-(dimethylamino)but-2-enoyl)azepan-3-yl)-1*H*-benzo[*d*]imidazol-2-yl)-2-methylisonicotinamide (47). A solution of **42** (8.62 g, 16.4 mmol) in MeOH (67 mL) was treated with HCl in dioxane (4 M, 67 mL), and the mixture was stirred at room temperature for 7 h. The mixture was then concentrated under reduced pressure to afford (*R*)-*N*-(1-(azepan-3-yl)-7-chloro-1*H*-benzo[*d*]imidazol-2-yl)-2-methylisonicotinamide (7.2 g) as the HCl salt. The product was used in the next step without further purification. A mixture of (*E*)-4-(dimethylamino)but-2-enoic acid hydrochloride (2.76 g, 21.4 mmol) and 1-ethyl-3-(3-dimethylaminopropyl)carbodiimide hydrochloride (4.10 g, 21.4 mmol) in DMF (80 mL) was treated with hydroxybenzotriazole (3.27 g, 21.4 mmol) and stirred at room temperature for 1 h. The resulting mixture was added to a solution of (*R*)-*N*-(1-(azepan-3-yl)-7-chloro-1*H*-benzo[*d*]imidazol-2-yl)-2-methylisonicotinamide (6.1 g, 13.4 mmol) in DMF (20 mL). Et_3N (13.0 mL, 93.5 mmol) was then added, and the mixture was stirred for 24 h. Water (2 mL) was added, and the mixture was concentrated under reduced pressure. The residue was diluted with water (250 mL) and extracted with EtOAc (3 × 200 mL). The combined organic layers were washed with water (100 mL), $NaHCO_3$ (100 mL), and brine (2 × 50 mL), dried over Na_2SO_4, filtered, and concentrated under reduced pressure. The crude was purified by column chromatography (0−100% (9:1:0.175N CH_2Cl_2/MeOH/NH_3)/CH_2Cl_2 gradient) to afford **47** (3.67 g, 56%). ^{1}H NMR (CD_3CN, 400 MHz): δ 12.55 (br s, 1H), 8.61 (d, J = 5.2 Hz, 1H), 7.98 (s, 0.6H), 7.95 (s, 0.4H), 7.88−7.85 (m, 1H), 7.53 (dd, J = 1.2, 8.0 Hz, 0.6H), 7.51 (dd, J = 1.2, 8.0 Hz, 0.4H), 7.33−7.23 (m, 2H), 6.81−6.72 (m, 1H), 6.60 (dt, J = 15.2, 1.6 Hz, 1H), 5.66−5.55 (m, 1H), 4.81−4.74 (m, 1H), 4.61−4.55 (m, 1H), 4.29−4.01 (m, 2H), 3.89−3.82 (m, 1H), 3.71−3.65 (m, 1H), 3.44−3.38 (m, 1H), 3.14 (d, J = 6.0 Hz, 1.2H), 2.92 (d, J = 6.0 Hz, 0.8H), 2.85−2.72 (m, 1H), 2.61 (d, J = 2.0 Hz, 3H), 2.27 (s, 6H), 2.16−2.00 (m, 1H), 1.52−1.41 (m, 1H). MS calculated for $C_{26}H_{32}ClN_6O_2$ $(M + H)^+$ 495.23, found 495.20. Anal. Calc. for $C_{26}H_{31}ClN_6O_2$ (495.02): C 63.09, H 6.31, N 16.98; found: C 62.90, H 6.21, N 16.90. $[\alpha]_D^{23}$ +53.76° (c 0.186, MeOH).

Molecular Docking Experiments. Flexible ligand docking was performed using Glide 6.5 (Schrodinger Inc., Portland, OR, 2014). The protein coordinates were taken from cocrystal structure of AEE788 with EGFR T790M mutant (PDB code 2jiu).[6] The grid box was centered on the cocrystallized ligand and extended 10 Å from the center, with the outer box extending an additional 20 Å. The ligand was docked using the standard precision (SP) algorithm, and during docking, constraints were imposed, requiring at least one H-bonding contact in the hinge region. The final pose was selected based on the lowest docking score using GlideScore.

Cloning, Expression, and Purification. DNA encoding the kinase domain of human WT EGFR (residues 696−1022) was amplified by PCR from a cDNA template and cloned into pFastBACHTb (Life Technologies) in-frame with the N-terminal 6xHIS tag and TEV (Tobacco Etch Virus) protease cleavage site. The T790M mutation was created using site-directed mutagenesis (QuikChange, Agilent Technologies). Bacmids were created via standard methods and transfected into Sf9 cells to generate recombinant baculovirus. Large scale expression of protein was also carried out in Sf9 cells with cultures being infected at a cell density of 1 × 10^6 cells/mL. The culture was harvested by centrifugation when cell viability reached 50% (~3−4 days post-transfection), and cell pellets were stored at −80 °C.

To purify the proteins (WT or T790M mutant), the cell pellets were resuspended in lysis buffer containing 20 mM Tris, pH 8.0, 150 mM NaCl, 2 mM TCEP, 5% v/v glycerol, and protease inhibitor cocktail tablets without EDTA (Roche). Cells were lysed by sonication, and the lysate was cleared by centrifugation at 20 000g at 4 °C for 45 min. The clarified lysate was applied to a 5 mL Ni-NTA column pre-equilibrated with lysis buffer. The bound protein was washed with lysis buffer supplemented with 20 mM imidazole. Bound protein was then eluted with lysis buffer supplemented with 300 mM imidazole. Fractions containing protein were combined and desalted into 20 mM Tris, pH 8.0, 50 mM NaCl, 2 mM TCEP using a PD10 column (GE Healthcare). To remove the 6xHIS tag, TEV protease was added to the desalted fractions at a ratio of 1 mg of TEV/20 mg of fusion protein and incubated at 4 °C overnight. Following overnight digest, the cleaved protein was applied to Ni-NTA resin to remove uncleaved protein, the flow through was collected and concentrated to 6 mg/mL. Aliquots were flash frozen in liquid nitrogen and stored at −80 °C.

Crystallization and Data Collection. Crystallization experiments were carried out using the sitting-drop vapor diffusion setup. The protein drug complex was formed by incubating the concentrated protein (WT EGFR kinase domain or T790M mutant) with 2 mM $MgCl_2$ and 0.5 mM drug (either racemic **43** or **46** from 10 mM DMSO stock). After addition of the inhibitor, the solution was incubated at room temperature for 90 min prior to crystallization plate setup. Crystallization plates were incubated at 20 °C. After 1−2 weeks, crystals of the EGFR T790M-**43** complex were visible in a well containing 1.2 M potassium sodium tartrate, 0.1 M HEPES, pH 7.5. Crystals of the EGFR T790M-**46** complex were visible in a well containing 32% v/v PEG 3350, 0.2 M lithium sulfate, 0.1 M HEPES, pH 7.25. Crystals of the WT EGFR-**43** complex grew out of a well containing 1.35 M potassium sodium tartrate, 0.1 M HEPES, pH 7.9. Crystals were cryopreserved in reservoir solution supplemented with 20% v/v ethylene glycol and flash frozen in liquid nitrogen prior to data collection. X-ray diffraction data were collected from frozen crystals on ALS beamline 5.0.3.

Structure Determination and Refinement. Diffraction data were processed using HKL2000,[45] and structures were solved by molecular replacement using PHASER.[46] Structure refinement was carried out in PHENIX[47] alternated with manual fitting in Coot.[48] Selection of TLS groups was carried out using the automated procedure implemented in PHENIX. Refinement statistics for cocrystals with **43** and **46** are included in the Supporting Information.

EGFR Biochemical Assays. Biochemical assays for WT EGFR and each mutant were carried out using a homogeneous time-resolved fluorescence (HTRF) assay as described previously.[49] Assays were optimized for each ATP concentration. Assays were carried out with or without 90 min enzyme/compound preincubation step. Compound IC_{50} values were determined by 12-point inhibition curves (from 50 to 0.000282 μM) in duplicate.

H1975, H3255, HCC827, and HaCaT Cellular EGFR Target Modulation Assays. Tissue culture cells were maintained in 10% FBS/RPMI supplemented with 100 μg/mL penicillin/streptomycin (Hyclone no. SH30236.01). The cells were harvested with 0.25% trypsin/EDTA (Hyclone no. SH30042.1), resuspended in 5% FBS/RPMI Pen/Strep, and plated at 7500 cells per well in 50 μL of medium in a 384-well black plate with clear bottoms (Greiner no. 789068G). The cells were allowed to incubate overnight in a 37 °C, 5% CO_2 humidified tissue culture incubator. The 12-point serial diluted test compounds were transferred to the plate containing cells by using a 50 nL Pin Head device (PerkinElmer), and the cells were placed back in the incubator for 3 h.

Phospho-EGFR (Y1173) target modulation assay HaCaT cells were stimulated with 10 ng/mL EGF (Peprotech no. AF-100-15) for 5 min at room temperature. Constitutively activated EGFR mutant cell lines (H1975, H3255, and HCC827) were not stimulated with EGF. The medium was reduced to 20 μL using a Bio-Tek ELx 405 Select plate washer. Cells were lysed with 20 μL of 2× lysis buffer containing protease and phosphatase inhibitors (2% Triton X-100, 40 mM Tris, pH 7.5, 2 mM EDTA, 2 mM EGTA, 300 mM NaCl, 2× complete cocktail inhibitor (Roche no. 11 697 498 001), 2× phosphatase inhibitor cocktail set II and set III (Sigma no. P5726 and no. P0044)). The plates were shaken for 20 min. An aliquot of 25 μL from each well was transferred to prepared ELISA plates for analysis.

Phospho-EGFR (Y1173) ELISA solid white 384-well high-binding ELISA plates (Greiner no. 781074) were coated with 5 μg/mL goat anti-EGFR capture antibody overnight in 50 mM

DOI: 10.1021/acs.jmedchem.5b01985
J. Med. Chem. 2016, 59, 6671−6689

carbonate/bicarbonate pH 9.5 buffer. Plates were blocked with 1% BSA (Sigma no. A7030) in PBS for 1 h at room temperature, and washes were carried out with a Bio-Tek ELx405 Select using 4 cycles of 100 μL of TBS-T (20 mM Tris, 137 mM NaCl, 0.05% Tween-20) per well. A 25 μL aliquot of lysed cell was added to each well of the ELISA plate and incubated overnight at 4 °C with gentle shaking. A 1:1000 anti-phospho-EGFR in 0.2% BSA/TBS-T was added and incubated for 2 h at room temperature. After washing, 1:2000 anti-rabbit-HRP in 0.2% BSA/TBS-T was added and incubated for 1 h at room temperature. Chemiluminescent detection was carried out with SuperSignal ELISA Pico substrate. Signal was read on EnVision plate reader using built-in UltraLUM setting.

In Vivo Efficacy Studies. Foxn1 nude mice bearing the H1975 tumors were randomized and used for efficacy studies. Compounds were formulated in 0.5% MC, 0.5% Tween80 suspension formulation and administered by oral gavage at a dosing volume of 10 μL/g of the animal body weight. Animals in each group received one oral dose of either vehicle ($n = 6$) or the different test compounds ($n = 6$ in each dose group). Plasma samples were collected for PK measurements at 30 min, 3 h, 7 h, and 24 h after last dose on day 5. Body weight was monitored daily, and the % change in body weight was calculated as $[(BW_{current} - BW_{initial})/(BW_{initial})] \times 100$. Data are presented as percent body weight change from the day of treatment initiation. Tumor sizes were assessed three times during the efficacy study for 5 days. Tumor sizes were determined by using caliper measurements. Tumor volumes were calculated with the formula (length × width × width)/2.

Percent treatment/control (T/C) values for tumor were calculated using the following formula: % $T/C = 100 \times \Delta T/\Delta C$ if $\Delta T > 0$; % regression = $100 \times \Delta T/T_{initial}$ if $\Delta T < 0$; where T is the mean tumor volume of the drug-treated group on the final day of the study; ΔT is mean tumor volume of the drug-treated group on the final day of the study minus mean tumor volume of the drug-treated group on initial day of dosing; $T_{initial}$ is the mean tumor volume of the drug-treated group on initial day of dosing; C is the mean tumor volume of the control group on the final day of the study; and ΔC is mean tumor volume of the control group on the final day of the study minus mean tumor volume of the control group on initial day of dosing.

All data were expressed as mean ± standard error of the mean (SEM). The Δ tumor volume and body weight were used for statistical analysis. Between groups comparisons were carried out using a one-way ANOVA followed by a post hoc Tukey or Dunn's. For all statistical evaluations the level of significance was set at $p < 0.05$. Significance compared to the vehicle control group is reported unless otherwise stated.

PK Studies. Rodent PK studies of **43**–**47** were conducted in male balb/c mice and male Wistar rats. Plasma concentrations of compounds were determined by liquid chromatography–tandem mass spectrometry (Applied Biosystems, Foster City, CA, USA). The lower limit of detection was 1 ng/mL. Pharmacokinetic parameters were calculated by noncompartmental regression analysis using an in-house fitting program.

In Vitro Adducts of 47 with EGFR. Recombinant kinase domain of EGFR L858R and T790M-L858R mutants were incubated with **47** to confirm covalent modification of EGFR and site of adduction. Recombinant enzyme was incubated at room temperature with a 20-fold molar excess of compound in 40 mM Tris, pH 8, 500 mM NaCl, 1% glycerol, 5 mM TCEP for 1 h. The reaction was quenched by addition of dithiothreitol (DTT, 80-fold excess to compound) and transfer to ice. A third of the reaction (10 μL) was processed for intact MS by adding an equal volume of 6 M Guan HCl, 100 mM Tris, pH 8, 20 mM DTT, 10 mM TCEP and incubating at room temperature for 15 min. Intact MS analysis was performed on an Agilent 6520 QToF mass spectrometer equipped with a dual spray ion source (IS of 4500 V, fragmentor of 250 V, fas temp of 350 °C, and skimmer of 75 V). The samples were injected onto a PLRP-S column (2.1 mm × 50 mm, Agilent), heated to 60 °C, and desalted for 2 min at 500 μL/min and 3% B prior to elution with a fast gradient of 3–50% B in 3 min (B, 0.1% formic acid, MeCN). The data were analyzed in MassHunter for automatic peak selection, integration, and spectral deconvolution with a mass range of 15 000–75 000 Da.

Reaction solutions were also processed for enzymatic digestion and LC/MSMS. Samples were buffer exchanged to remove excess compound using 10 kDa Amicon Ultra 0.5 mL spin filters and recovered in 30 μL of 100 mM Tris, pH 8, 20 mM DTT and incubated at 60 °C for 20 min. Iodoacetamide was added to 25 mM, and the samples were incubated for 45 min at room temperature in the dark prior to dilution to 150 μL with 100 mM Tris, pH 8, 10 mM DTT. The samples were divided in two, and 1 μL of either 0.5 mg/mL chymotrypsin or sequencing grade modified trypsin was added and incubated overnight at 37 °C. Samples were acidified to 1% formic acid and analyzed on a Q-Exactive mass spectrometer for accurate mass and MS/MS. Samples were injected on a precolumn (360 μm × 100 μm, 4 cm Poros10R2) for desalting and separated on a 360 μm × 75 μm analytical column and integrated emitter (10 cm, 5 μm Monitor C18) with a gradient of 2–27% B in 45 min; 27–36% B in 10 min at a flow rate of 300 nL/min (B, 0.1% formic acid, MeCN). The Q-Exactive parameters were set for "sensitive" analysis as previously defined by Kelstrup et al.[50] Briefly, one full scan MS was acquired at 75 000 resolution followed by 12 MS/MS at 35 000 resolution of the top ions in the mass range of 350–1500 m/z. An additional dedicated scan for MS/MS of 898.7184 was added to continuously target the adduct Cys797. The data were converted to Mascot generic format (MGF) using Proteome Discoverer (Thermo) and searched using Mascot against a custom database allowing for variable modification of methionine oxidation, cysteine carbamidomethylation, and the custom modification of Michael addition by **47** to cysteines. Enzyme specificity was trypsin or no enzyme (chymotrypsin digest), and the peptide and fragment ion tolerances were set to 25 ppm and 50 mmu, respectively. The data were visualized in Scaffold 4.4.3 and filtered for 95% peptide confidence and 99% protein confidence.

■ ASSOCIATED CONTENT

Supporting Information

The Supporting Information is available free of charge on the ACS Publications website at DOI: 10.1021/acs.jmedchem.5b01985.

Refinement statistics of cocrystal structures WT-EGFR-**43**, EGFR T790M-**43** and EGFR T790M-**46**; biochemical selectivity profiling of **47** against a panel of kinase and non-kinase targets; enantiopurity analysis of chiral compounds; analytical LC–MS methods for analysis of intermediates; metabolite identification studies for **43**; ^{1}H and ^{13}C NMR spectra of **47** at 300 and 383 K (PDF)

Molecular formula strings and some data (CSV)

Accession Codes

The crystallographic coordinates and structure factors have been deposited in the Protein Data Bank, www.pdb.org (PDB codes 5fee for EGFR T790M-**43**, 5fed for WT EGFR-**43**, and 5feq for EGFR T790M-**46**).

■ AUTHOR INFORMATION

Corresponding Author

*Phone: +1-858-332-4452; e-mail: glelais@gnf.org.

Present Address

‖R.F.: Genentech, 1 DNA Way, South San Francisco, CA 94080, U.S.

Notes

The authors declare no competing financial interest.

■ ACKNOWLEDGMENTS

The authors acknowledge the contribution to this work of all past and present members of the mutant EGFR team. A big thank you goes also to all supporting functions including Paul

DOI: 10.1021/acs.jmedchem.5b01985
J. Med. Chem. 2016, 59, 6671–6689

Calvin and his team (compound management), Thomas Hollenbeck and his team (analytical group), Lucas Westling (chiral analysis and purifications), David Jones (NMR), Connie Chen (protein crystallization), and Tove Tuntland and her team (DMPK).

■ ABBREVIATIONS USED

MoA, mode of action; OS, overall survival; HT-sol, high-throughput solubility; HTRF, homogeneous time-resolved fluorescence; GSH, glutathione; CL, clearance; LipE, lipophilic efficiency; *T*/*C*, treatment/control; Da, dalton; RP-HPLC, reverse phase high-performance liquid chromatography; PDA, photodiode array detector; ELSD, evaporative light scattering detector; DIPEA, *N*,*N*-diisopropylethylamine

■ REFERENCES

(1) Sharma, S. V.; Bell, D. W.; Settleman, J.; Haber, D. A. Epidermal growth factor receptor mutations in lung cancer. *Nat. Rev. Cancer* **2007**, *7*, 169−181.

(2) Paez, J. G.; Jänne, P. A.; Lee, J. C.; Tracy, S.; Greulich, H.; Gabriel, S.; Herman, P.; Kaye, F. J.; Lindeman, N.; Boggon, T. J.; Naoki, K.; Sasaki, H.; Fujii, Y.; Eck, M. J.; Sellers, W. R.; Johnson, B. E.; Meyerson, M. EGFR mutations in lung cancer: correlation with clinical response to gefitinib therapy. *Science* **2004**, *304*, 1497−1500.

(3) Köhler, J.; Schuler, M. Afatinib, erlotinib and gefitinib in the first-line therapy of EGFR mutation-positive lung adenocarcinoma: a review. *Onkologie* **2013**, *36*, 510−518.

(4) Pao, W.; Miller, V. A.; Politi, K. A.; Riely, G. J.; Somwar, R.; Zakowski, M. F.; Kris, M. G.; Varmus, H. Acquired resistance of lung adenocarcinomas to gefitinib or erlotinib is associated with a second mutation in the EGFR kinase domain. *PLoS Med.* **2005**, *2*, e73.

(5) Sequist, L. V.; Waltman, B. A.; Dias-Santagata, D.; Digumarthy, S.; Turke, A. B.; Fidias, P.; Bergethon, K.; Shaw, A. T.; Gettinger, S.; Cosper, A. K.; Akhavanfard, S.; Heist, R. S.; Temel, J.; Christensen, J. G.; Wain, J. C.; Lynch, T. J.; Vernovsky, K.; Mark, E. J.; Lanuti, M.; Iafrate, A. J.; Mino-Kenudson, M.; Engelman, J. A. Genotypic and histological evolution of lung cancers acquiring resistance to EGFR inhibitors. *Sci. Transl. Med.* **2011**, *3*, 75ra26.

(6) Yun, C.-H.; Mengwasser, K. E.; Toms, A. V.; Woo, M. S.; Greulich, H.; Wong, K.-K.; Meyerson, M.; Eck, M. J. The T790M mutation in EGFR kinase causes drug resistance by increasing the affinity for ATP. *Proc. Natl. Acad. Sci. U. S. A.* **2008**, *105*, 2070−2075.

(7) Li, D.; Ambrogio, L.; Shimamura, T.; Kubo, S.; Takahashi, M.; Chirieac, L. R.; Padera, R. F.; Shapiro, G. I.; Baum, A.; Himmelsbach, F.; Rettig, W. J.; Meyerson, M.; Solca, F.; Greulich, H.; Wong, K.-K. BIBW2992, an irreversible EGFR/HER2 inhibitor highly effective in preclinical lung cancer models. *Oncogene* **2008**, *27*, 4702−4711.

(8) Gonzales, A. J.; Hook, K. E.; Althaus, I. W.; Ellis, P. A.; Trachet, E.; Delaney, A. M.; Harvey, P. J.; Ellis, T. A.; Amato, D. M.; Nelson, J. M.; Fry, D. W.; Zhu, T.; Loi, C.-M.; Fakhoury, S. A.; Schlosser, K. M.; Sexton, K. E.; Winters, R. T.; Reed, J. E.; Bridges, A. J.; Lettiere, D. J.; Baker, D. A.; Yang, J.; Lee, H. T.; Tecle, H.; Vincent, P. W. Antitumor activity and pharmacokinetic properties of PF-00299804, a second-generation irreversible pan-erbB receptor tyrosine kinase inhibitor. *Mol. Cancer Ther.* **2008**, *7*, 1880−1889.

(9) Engelman, J. A.; Zejnullahu, K.; Gale, C.-M.; Lifshits, E.; Gonzales, A. J.; Shimamura, T.; Zhao, F.; Vincent, P. W.; Naumov, G. N.; Bradner, J. E.; Althaus, I. W.; Gandhi, L.; Shapiro, G. I.; Nelson, J. M.; Heymach, J. V.; Meyerson, M.; Wong, K.-K.; Jänne, P. A. PF00299804, an irreversible pan-ERBB inhibitor, is effective in lung cancer models with EGFR and ERBB2 mutations that are resistant to gefitinib. *Cancer Res.* **2007**, *67*, 11924−11932.

(10) Smaill, J. B.; Rewcastle, G. W.; Loo, J. A.; Greis, K. D.; Chan, O. H.; Reyner, E. L.; Lipka, E.; Showalter, H. D. H.; Vincent, P. W.; Elliott, W. L.; Denny, W. A. Tyrosine kinase inhibitors. 17. Irreversible inhibitors of the epidermal growth factor receptor: 4-(phenylamino)-quinazoline- and 4-(phenylamino)pyrido[3,2-*d*]pyrimidine-6-acrylamides bearing additional solubilizing functions. *J. Med. Chem.* **2000**, *43*, 1380−1397.

(11) Fry, D. W.; Bridges, A. J.; Denny, W. A.; Doherty, A.; Greis, K. D.; Hicks, J. L.; Hook, K. E.; Keller, P. R.; Leopold, W. R.; Loo, J. A.; McNamara, D. J.; Nelson, J. M.; Sherwood, V.; Smaill, J. B.; Trumpp-Kallmeyer, S.; Dobrusin, E. M. Specific, irreversible inactivation of the epidermal growth factor receptor and erbB2, by a new class of tyrosine kinase inhibitor. *Proc. Natl. Acad. Sci. U. S. A.* **1998**, *95*, 12022−12027.

(12) Solca, F.; Dahl, G.; Zoephel, A.; Bader, G.; Sanderson, M.; Klein, C.; Kraemer, O.; Himmelsbach, F.; Haaksma, E.; Adolf, G. R. Target binding properties and cellular activity of afatinib (BIBW 2992), an irreversible ErbB family blocker. *J. Pharmacol. Exp. Ther.* **2012**, *343*, 342−350.

(13) Kim, Y.; Ko, J.; Cui, Z.; Abolhoda, A.; Ahn, J. S.; Ou, S.-H.; Ahn, M.-J.; Park, K. The EGFR T790M mutation in acquired resistance to an irreversible second-generation EGFR inhibitor. *Mol. Cancer Ther.* **2012**, *11*, 784−791.

(14) Yu, H. A.; Pao, W. Targeted therapies: Afatinib - new therapy option for EGFR-mutant lung cancer. *Nat. Rev. Clin. Oncol.* **2013**, *10*, 551−552.

(15) Zhou, W.; Ercan, D.; Chen, L.; Yun, C.-H.; Li, D.; Capelletti, M.; Cortot, A. B.; Chirieac, L.; Iacob, R. E.; Padera, R.; Engen, J. R.; Wong, K.-K.; Eck, M. J.; Gray, N. S.; Jänne, P. A. Novel mutant-selective EGFR kinase inhibitors against EGFR T790M. *Nature* **2009**, *462*, 1070−1074.

(16) Chang, S.; Zhang, L.; Xu, S.; Luo, J.; Lu, X.; Zhang, Z.; Xu, T.; Liu, Y.; Tu, Z.; Xu, Y.; Ren, X.; Geng, M.; Ding, J.; Pei, D.; Ding, K. Design, synthesis, and biological evaluation of novel conformationally constrained inhibitors targeting epidermal growth factor receptor threonine790 –> methionine790 mutant. *J. Med. Chem.* **2012**, *55*, 2711−2723.

(17) Zhou, W.; Ercan, D.; Jänne, P. A.; Gray, N. S. Discovery of selective irreversible inhibitors for EGFR-T790M. *Bioorg. Med. Chem. Lett.* **2011**, *21*, 638−643.

(18) Xu, S.; Zhang, L.; Chang, S.; Luo, J.; Lu, X.; Tu, Z.; Liu, Y.; zhang, Z.; Xu, Y.; Ren, X.; Ding, K. Design, synthesis and biological evaluation of new molecules inhibiting epidermal growth factor receptor threonine790→ methionine790 mutant. *MedChemComm* **2012**, *3*, 1155.

(19) Xu, T.; Zhang, L.; Xu, S.; Yang, C.-Y.; Luo, J.; Ding, F.; Lu, X.; Liu, Y.; Tu, Z.; Li, S.; Pei, D.; Cai, Q.; Li, H.; Ren, X.; Wang, S.; Ding, K. Pyrimido[4,5-d]pyrimidin-4(1H)-one derivatives as selective inhibitors of EGFR threonine790 to methionine790 (T790M) mutants. *Angew. Chem., Int. Ed.* **2013**, *52*, 8387−8390.

(20) Finlay, M. R. V.; Anderton, M.; Ashton, S.; Ballard, P.; Bethel, P. A.; Box, M. R.; Bradbury, R. H.; Brown, S. J.; Butterworth, S.; Campbell, A.; Chorley, C.; Colclough, N.; Cross, D. A. E.; Currie, G. S.; Grist, M.; Hassall, L.; Hill, G. B.; James, D.; James, M.; Kemmitt, P.; Klinowska, T.; Lamont, G.; Lamont, S. G.; Martin, N.; McFarland, H. L.; Mellor, M. J.; Orme, J. P.; Perkins, D.; Perkins, P.; Richmond, G.; Smith, P.; Ward, R. A.; Waring, M. J.; Whittaker, D.; Wells, S.; Wrigley, G. L. Discovery of a potent and selective EGFR inhibitor (AZD9291) of both sensitizing and T790M resistance mutations that spares the wild type form of the receptor. *J. Med. Chem.* **2014**, *57*, 8249−8267.

(21) Ward, R. A.; Anderton, M. J.; Ashton, S.; Bethel, P. A.; Box, M.; Butterworth, S.; Colclough, N.; Chorley, C. G.; Chuaqui, C.; Cross, D. A. E.; Dakin, L. A.; Debreczeni, J. E.; Eberlein, C.; Finlay, M. R. V.; Hill, G. B.; Grist, M.; Klinowska, T. C. M.; Lane, C.; Martin, S.; Orme, J. P.; Smith, P.; Wang, F.; Waring, M. J. Structure- and reactivity-based development of covalent inhibitors of the activating and gatekeeper mutant forms of the epidermal growth factor receptor (EGFR). *J. Med. Chem.* **2013**, *56*, 7025−7048.

(22) Singh, J.; Evans, E.; Hagel, M.; Labinski, M.; Dubrovskiy, A.; Nacht, M.; Petter, R. C.; Prasad, A.; Sheets, M.; St Martin, T.; Tjin Tham Sjin, R.; Westlin, W.; Zhu, Z. Superiority of a novel EGFR targeted covalent inhibitor over its reversible counterpart in overcoming drug resistance. *MedChemComm* **2012**, *3*, 780.

(23) Cross, D. A.; Ashton, S. E.; Ghiorghiu, S.; Eberlein, C.; Nebhan, C. A.; Spitzler, P. J.; Orme, J. P.; Finlay, M. R. V.; Ward, R. A.; Mellor,

DOI: 10.1021/acs.jmedchem.5b01985
J. Med. Chem. 2016, 59, 6671−6689

M. J.; Hughes, G.; Rahi, A.; Jacobs, V. N.; Red Brewer, M.; Ichihara, E.; Sun, J.; Jin, H.; Ballard, P.; Al-Kadhimi, K.; Rowlinson, R.; Klinowska, T.; Richmond, G. H.; Cantarini, M.; Kim, D.-W.; Ranson, M. R.; Pao, W. AZD9291, an irreversible EGFR TKI, overcomes T790M-mediated resistance to EGFR inhibitors in lung cancer. *Cancer Discovery* **2014**, *4*, 1046−1061.

(24) FDA approves new pill to treat certain patients with non-small cell lung cancer. http://www.fda.gov/NewsEvents/Newsroom/PressAnnouncements/ucm472525.htm (accessed November 13, 2015).

(25) Walter, A. O.; Sjin, R. T. T.; Haringsma, H. J.; Ohashi, K.; Sun, J.; Lee, K.; Dubrovskiy, A.; Labenski, M.; Zhu, Z.; Wang, Z.; Sheets, M.; St Martin, T.; Karp, R.; van Kalken, D.; Chaturvedi, P.; Niu, D.; Nacht, M.; Petter, R. C.; Westlin, W.; Lin, K.; Jaw-Tsai, S.; Raponi, M.; Van Dyke, T.; Etter, J.; Weaver, Z.; Pao, W.; Singh, J.; Simmons, A. D.; Harding, T. C.; Allen, A. Discovery of a mutant-selective covalent inhibitor of EGFR that overcomes T790M-mediated resistance in NSCLC. *Cancer Discovery* **2013**, *3*, 1404−1415.

(26) Tjin Tham Sjin, R.; Lee, K.; Walter, A. O.; Dubrovskiy, A.; Sheets, M.; Martin, T. S.; Labenski, M. T.; Zhu, Z.; Tester, R.; Karp, R.; Medikonda, A.; Chaturvedi, P.; Ren, Y.; Haringsma, H.; Etter, J.; Raponi, M.; Simmons, A. D.; Harding, T. C.; Niu, D.; Nacht, M.; Westlin, W. F.; Petter, R. C.; Allen, A.; Singh, J. In vitro and in vivo characterization of irreversible mutant-selective EGFR inhibitors that are wild-type sparing. *Mol. Cancer Ther.* **2014**, *13*, 1468−1479.

(27) Jänne, P. A.; Yang, J. C.-H.; Kim, D.-W.; Planchard, D.; Ohe, Y.; Ramalingam, S. S.; Ahn, M.-J.; Kim, S.-W.; Su, W.-C.; Horn, L.; Haggstrom, D.; Felip, E.; Kim, J.-H.; Frewer, P.; Cantarini, M.; Brown, K. H.; Dickinson, P. A.; Ghiorghiu, S.; Ranson, M. AZD9291 in EGFR inhibitor-resistant non-small-cell lung cancer. *N. Engl. J. Med.* **2015**, *372*, 1689−1699.

(28) Sequist, L. V.; Soria, J.-C.; Goldman, J. W.; Wakelee, H. A.; Gadgeel, S. M.; Varga, A.; Papadimitrakopoulou, V.; Solomon, B. J.; Oxnard, G. R.; Dziadziuszko, R.; Aisner, D. L.; Doebele, R. C.; Galasso, C.; Garon, E. B.; Heist, R. S.; Logan, J.; Neal, J. W.; Mendenhall, M. A.; Nichols, S.; Piotrowska, Z.; Wozniak, A. J.; Raponi, M.; Karlovich, C. A.; Jaw-Tsai, S.; Isaacson, J.; Despain, D.; Matheny, S. L.; Rolfe, L.; Allen, A. R.; Camidge, D. R. Rociletinib in EGFR-mutated non-small-cell lung cancer. *N. Engl. J. Med.* **2015**, *372*, 1700−1709.

(29) Novartis Pharmaceuticals. A phase I/II, multicenter, open-label study of EGFRmut-TKI EGF816, administered orally in adult patients with EGFRmut solid malignancies. NLM Identifier: NCT02108964. http://clinicaltrials.gov/show/NCT02108964 (cited December 16, 2015).

(30) Novartis Pharmaceuticals. Study of efficacy and safety of nivolumab in combination with EGF816 and of nivolumab in combination with INC280 in patients with previously treated non-small cell lung cancer. NLM Identifier: NCT02323126. http://clinicaltrials.gov/show/NCT02323126 (cited December 16, 2015).

(31) Novartis Pharmaceuticals. Study of safety and efficacy of EGF816 in combination with INC280 in non-small cell lung cancer patients with EGFR mutation. NLM Identifier: NCT02335944. http://clinicaltrials.gov/show/NCT02335944 (cited December 16, 2015).

(32) Jia, Y.; Manuia, M.; Juarez, J. HTRF kinase assay development and methods in inhibitor characterization. In *Methods in Molecular Biology*; Zegzouti, H., Gouell, S. A., Eds.; Humana Press: New York, 2016; Vol. *1360*, pp 1−18, DOI: 10.1007/978-1-4939-3073-9_1.

(33) Powers, J. P.; Li, S.; Jaen, J. C.; Liu, J.; Walker, N. P. C.; Wang, Z.; Wesche, H. Discovery and initial SAR of inhibitors of interleukin-1 receptor-associated kinase-4. *Bioorg. Med. Chem. Lett.* **2006**, *16*, 2842−2845.

(34) Wang, Z.; Liu, J.; Sudom, A.; Ayres, M.; Li, S.; Wesche, H.; Powers, J. P.; Walker, N. P. C. Crystal structures of IRAK-4 kinase in complex with inhibitors: a serine/threonine kinase with tyrosine as a gatekeeper. *Structure* **2006**, *14*, 1835−1844.

(35) Snow, R. J.; Abeywardane, A.; Campbell, S.; Lord, J.; Kashem, M. A.; Khine, H. H.; King, J.; Kowalski, J. A.; Pullen, S. S.; Roma, T.; Roth, G. P.; Sarko, C. R.; Wilson, N. S.; Winters, M. P.; Wolak, J. P.; Cywin, C. L. Hit-to-lead studies on benzimidazole inhibitors of ITK: discovery of a novel class of kinase inhibitors. *Bioorg. Med. Chem. Lett.* **2007**, *17*, 3660−3665.

(36) Wang, Z.; Sun, D.; Johnstone, S.; Cao, Z.; Gao, X.; Jaen, J. C.; Liu, J.; Lively, S.; Miao, S.; Sudom, A.; Tomooka, C.; Walker, N. P. C.; Wright, M.; Yan, X.; Ye, Q.; Powers, J. P. Discovery of potent, selective, and orally bioavailable inhibitors of interleukin-1 receptor-associate kinase-4. *Bioorg. Med. Chem. Lett.* **2015**, *25*, 5546−5550.

(37) Wissner, A.; Overbeek, E.; Reich, M. F.; Floyd, M. B.; Johnson, B. D.; Mamuya, N.; Rosfjord, E. C.; Discafani, C.; Davis, R.; Shi, X.; Rabindran, S. K.; Gruber, B. C.; Ye, F.; Hallett, W. A.; Nilakantan, R.; Shen, R.; Wang, Y.-F.; Greenberger, L. M.; Tsou, H.-R. Synthesis and structure-activity relationships of 6,7-disubstituted 4-anilinoquinoline-3-carbonitriles. The design of an orally active, irreversible inhibitor of the tyrosine kinase activity of the epidermal growth factor receptor (EGFR) and the human epidermal growth factor receptor-2 (HER-2). *J. Med. Chem.* **2003**, *46*, 49−63.

(38) Tsou, H.-R.; Overbeek-Klumpers, E. G.; Hallett, W. A.; Reich, M. F.; Floyd, M. B.; Johnson, B. D.; Michalak, R. S.; Nilakantan, R.; Discafani, C.; Golas, J.; Rabindran, S. K.; Shen, R.; Shi, X.; Wang, Y.-F.; Upeslacis, J.; Wissner, A. Optimization of 6,7-disubstituted-4-(arylamino)quinoline-3-carbonitriles as orally active, irreversible inhibitors of human epidermal growth factor receptor-2 kinase activity. *J. Med. Chem.* **2005**, *48*, 1107−1131.

(39) Zhang, X.; Gureasko, J.; Shen, K.; Cole, P. A.; Kuriyan, J. An allosteric mechanism for activation of the kinase domain of epidermal growth factor receptor. *Cell* **2006**, *125*, 1137−1149.

(40) Richmond, W.; Wogan, M.; Isbell, J.; Gordon, W. P. Interstrain differences of in vitro metabolic stability and impact on early drug discovery. *J. Pharm. Sci.* **2010**, *99*, 4463−4468.

(41) Ryckmans, T.; Edwards, M. P.; Horne, V. A.; Correia, A. M.; Owen, D. R.; Thompson, L. R.; Tran, I.; Tutt, M. F.; Young, T. Rapid assessment of a novel series of selective CB(2) agonists using parallel synthesis protocols: A Lipophilic Efficiency (LipE) analysis. *Bioorg. Med. Chem. Lett.* **2009**, *19*, 4406−4409.

(42) Yun, C.-H.; Boggon, T. J.; Li, Y.; Woo, M. S.; Greulich, H.; Meyerson, M.; Eck, M. J. Structures of lung cancer-derived EGFR mutants and inhibitor complexes: mechanism of activation and insights into differential inhibitor sensitivity. *Cancer Cell* **2007**, *11*, 217−227.

(43) Jia, Y.; Juarez, J.; Li, J.; Manuia, M.; Niederst, M. J.; Tompkins, C.; Timple, N.; Vaillancourt, M. T.; Pferdekamper, A. C.; Lockerman, E. L.; Li, C.; Anderson, J.; Costa, C.; Liao, D.; Murphy, E.; DiDonato, M.; Bursulaya, B.; Lelais, G.; Barretina, J.; McNeill, M.; Epple, R.; Marsilje, T. H.; Pathan, N.; Engelman, J. A.; Michellys, P. Y.; McNamara, P.; Harris, J.; Bender, S.; Kasibhatla, S. EGF816 exerts anticancer effects in non-small cell lung cancer by irreversibly and selectively targeting primary and acquired activating mutations in the EGF receptor. *Cancer Res.* **2016**, *76*, 1591−1602.

(44) Tan, D. S.-W.; Seto, T.; Leighl, N. B.; Riely, G. J.; Sequist, L. V.; Felip, E.; Wolf, J.; Yang, J. C.-H.; Matushansky, I.; Yu, X.; Hsu Schmitz, S.-F.; Cui, X.; Kim, D.-W. First-in-human phase I study of EGF816, a third generation, mutant-selective EGFR tyrosine kinase inhibitor, in advanced non-small cell lung cancer (NSCLC) harboring T790M. *J. Clin. Oncol.* **2015**, *33* (Suppl.), 8013.

(45) Otwinowski, Z.; Minor, W. Processing of X-ray diffraction data collected in oscillation mode. *Methods Enzymol.* **1997**, *276*, 307−326.

(46) McCoy, A. J.; Grosse-Kunstleve, R. W.; Adams, P. D.; Winn, M. D.; Storoni, L. C.; Read, R. J. Phaser crystallographic software. *J. Appl. Crystallogr.* **2007**, *40*, 658−674.

(47) Afonine, P. V.; Grosse-Kunstleve, R. W.; Echols, N.; Headd, J. J.; Moriarty, N. W.; Mustyakimov, M.; Terwilliger, T. C.; Urzhumtsev, A.; Zwart, P. H.; Adams, P. D. Towards automated crystallographic structure refinement with phenix.refine. *Acta Crystallogr., Sect. D: Biol. Crystallogr.* **2012**, *68*, 352−367.

(48) Emsley, P.; Lohkamp, B.; Scott, W. G.; Cowtan, K. Features and development of Coot. *Acta Crystallogr., Sect. D: Biol. Crystallogr.* **2010**, *66*, 486−501.

DOI: 10.1021/acs.jmedchem.5b01985
J. Med. Chem. 2016, 59, 6671−6689

(49) Hong, L.; Quinn, C. M.; Jia, Y. Evaluating the utility of the HTRF Transcreener ADP assay technology: a comparison with the standard HTRF assay technology. *Anal. Biochem.* **2009**, *391*, 31−38.
(50) Kelstrup, C. D.; Young, C.; Lavallee, R.; Nielsen, M. L.; Olsen, J. V. Optimized fast and sensitive acquisition methods for shotgun proteomics on a quadrupole orbitrap mass spectrometer. *J. Proteome Res.* **2012**, *11*, 3487−3497.

DOI: 10.1021/acs.jmedchem.5b01985
J. Med. Chem. 2016, 59, 6671−6689